To appear in *Structure and Infrastructure Engineering*
Vol. 00, No. 00, Month 20XX, 1–31

Original Paper

On the vertical coupling effect of ballasted tracks in multi–span simply–supported railway bridges under operating conditions

Emma Moliner[a,*], Maria Dolores Martínez-Rodrigo[a], Pedro Galvín[b,c], Josep Chordà-Monsonís[a,b], Antonio Romero[b]

[a] *Universitat Jaume I, Department of Mechanical Engineering and Construction, Avda. Sos Baynat s/n, ES-12071 Castellón, Spain*

[b] *Escuela Técnica Superior de Ingeniería, Universidad de Sevilla, Camino de los Descubrimientos, ES-41092 Sevilla, Spain*

[c] *ENGREEN, Laboratory of Engineering for Energy and Environmental Sustainability, Universidad de Sevilla, Camino de los Descubrimientos, ES-41092 Sevilla, Spain*

(*Received 00 Month 20XX; final version received 00 Month 20XX*)

Abstract
This contribution investigates the vertical coupling exerted by ballasted tracks on the vertical response of bridges composed either of (i) several successive simply-supported spans with weak coupling between them due to the continuous track; or (ii) adjacent single-track decks conforming a double-track bridge, in which interaction effects are induced due to the transverse continuity of the ballast layer. To this end, 2D and 3D track-bridge interaction Finite Element models are implemented, which consider a three-layer discrete and explicit idealization of the track. The 2D track-bridge interaction model is used to perform sensitivity analyses on the track parameters, which have revealed that the ballast shear mechanisms along the track may significantly affect the train-induced vibrations under resonant conditions. Then, the influence of the ballast coupling on the response of twin adjacent decks is investigated with a 3D track-bridge interaction model. To this end, this model is updated based on the results of an experimental campaign performed on a real bridge composed of two SS spans and two single track twin adjacent decks. The numerical-experimental comparison shows an evident dynamic vertical coupling between the bridge decks and reveals the importance of including the ballasted track in the modelling process of these structures.

Keywords: Multispan railway bridges, ballasted track, track-structure interaction, span coupling, experimental measurements, resonance, vertical acceleration.

1. Introduction

The sustained development of transportation systems and, especially, railways for passenger and freight transport has set a milestone in most developed countries in recent decades. The progressive increase in the trains operational speeds and in the transportation capacity constitutes a challenge for infrastructures, which need to accomplish strict requirements to ensure the admissible levels of quality, safety and reliability. In particular, the Spanish railway network currently has a total of 135 km of track that runs over more than 6000 bridges. The dynamic effects on such structures, directly related with the vehicle velocity, have become an issue of interest and concern for scientists and engineers, especially since the advent of High-Speed (HS) (Frýba (2008)). An excessive level of vertical acceleration at the deck platform can lead to passenger discomfort, fatigue problems in the long term, to an increase of the maintenance costs of the lines, misalignment of the rails as a result

*Corresponding author. Email addresses: molinere@uji,es, mrodrigo@uji.es, pedrogalvin@us.es, jchorda@uji.es, aro@us.es

of premature deconsolidation of the ballast layer and even to the loss of contact between wheel and rail with the resultant increase of the risk of derailment. Consequently, the Serviceability Limit States for Traffic Safety and, in particular, the vertical acceleration at the deck has become one of the most restrictive requirements in the design of new bridges (CEN/TC250 (2005)). Bridges composed of simply–supported (SS) spans with short to medium span lengths are especially critical in this regard, which may become particularly relevant at resonance (Hoorpah (2008); Zacher and Baeþler (2008)).

Aside from the design of new structures, it is essential to realistically assess the performance of existing bridges when facing new traffic requirements. In this context, there is a need of (i) accurate and computationally efficient numerical models to predict the response, (ii) experimental data to provide up-to-date information on the condition of the structures, and (iii) appropriate analysis methodologies as essential tools for the decision–making process. However, the dynamic response of a bridge under the circulation of a train is complex and it is affected by several factors. The most obvious ones are the bridge geometrical and mechanical properties, the scheme of train axles, and the speed of circulation, being also the most certain (Rocha et al. (2012)). Additionally, there are other factors that are much more uncertain to determine that significantly affect the response of the bridge such as structural damping (Rocha et al. (2014)) and various interaction mechanisms which modelling is not trivial and is currently under investigation, being the most relevant vehicle–structure (Jahangiri and Zakeri (2017); Zakeri et al. (2014)), track–structure (Ticona et al. (2020); Zhai et al. (2019)) and soil–structure (Galvín et al. (2021); Zangeneh et al. (2019)) interaction. In engineering consultancies, simplified numerical models that generally disregard these mechanisms are most often used, given the uncertainties and the considerable computational cost involved in their modelling.

This work contributes to the investigation on the vertical coupling effect exerted by the ballasted track on railway bridges composed of SS spans in two situations: (i) in SS multi–span viaducts, where a weak coupling between consecutive spans occurs through the track (see Figure 1(a)-(b)); and (ii) in double–track bridges composed of two adjacent structurally independent decks, which vertical motion is coupled through the ballast, quite common in countries like Germany (Rauert et al. (2010)) and Spain (see Figure 1(c)-(d)). The contribution of the ballasted track to the dynamic response of the bridge remains a matter of recent investigation (Bornet et al. (2015); Melo et al. (2020); Rebelo et al. (2008)). A few authors have concluded from field measurements that the presence of the rail may influence the boundary conditions at the end sections where the track continuity introduces a moment of resistance (Rebelo et al. (2008); Rigueiro et al. (2006a,b)). According to some authors, this is one of the reasons for the discrepancies found between calculated and measured modal parameters in short or medium span bridges (Bornet et al. (2015)).

A few references can be found in the literature devoted to the coupling effect of the ballast over adjacent single-track decks in double-track bridges, and its influence on the dynamic response. Among them, Rebelo et al. (2008) presented the results of an experimental campaign on a number of single–span bridges of this typology. The authors pointed out that the coupling effect between twin slabs is particularly evident in skewed configurations, and attributed the high level of damping identified to this effect. They also pointed out the inherently non linear character of the interaction, resulting the stiffness associated to the ballast coupling higher for lower amplitudes of vibration. Rigueiro et al. (2010) compared the numerical predictions from a finite element (FE) plate model of two SS twin decks coupled through the ballast layer. Three discrete track models were compared. The authors concluded that for frequencies up to $10 - 15\,\mathrm{Hz}$ the influence of the track model is minor, but for higher frequencies the track acts as a filter. These authors also expressed the need to investigate the response of such structures at resonance. Rauert et al. (2010) presented an intense experimental campaign where the load transfer mechanism between ballast-connected structures as well as the contribution of the ballast layer to the global bending stiffness of SS bridges were investigated. The authors showed that ballast–coupled bridge decks provide a considerable amount of additional stiffness, particularly during train passages. Bonifácio et al. (2014) assessed the dynamic behaviour of a short span filler-beam railway bridge composed of two independent

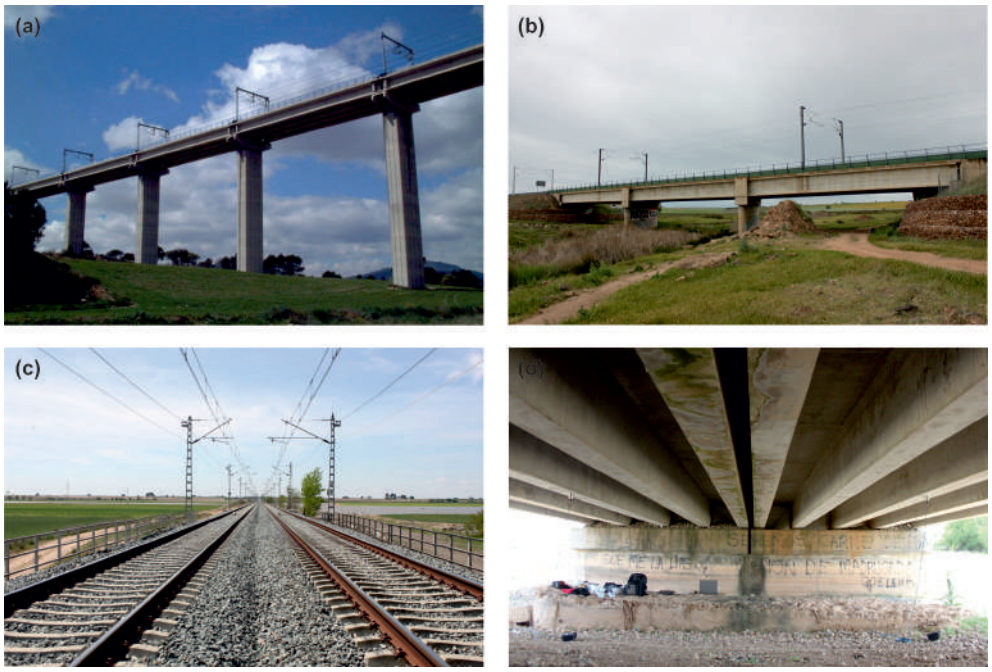

Figure 1. (a)-(b) SS multi–span railway viaducts in Spanish HS lines; (c)-(d) railway bridge in Spanish conventional line composed of two adjacent structurally independent decks.

decks and several SS spans subjected to the TGV-double train. They pointed out an obvious coupling between the spans in the mode shapes and an important transfer of vibrations from the loaded to the unloaded deck under operational conditions.

Fewer still are the works found in the literature devoted to the so–called weak coupling induced by the track between successive spans in SS viaducts. Among them, Chellini et al. (2011) presented the experimental identification of modal parameters in two steel-concrete composite viaducts of the Torino-Milano HS line in Italy. The work reveals a clear dynamic interaction between the spans. The authors implemented a 3D FE comprehensive numerical model of a single span of each bridge and introduce artificial boundary conditions between the spans in order to reproduce the continuity of the tracks, which is found to be essential. Liu et al. (2014) evaluated the dynamic response of multi–span SS viaducts. The authors implemented and calibrated two numerical models to take into account this effect: a single-span model with modified boundary conditions and a component synthesis model (CMS) or reduced order model of the entire viaduct. A better representation of the vertical acceleration of the viaduct was obtained with the CMS model at a reasonable computational cost. Finally, Bornet et al. (2015) performed experimental tests on a SS single-span single-track steel truss railway bridge before and after the ballasted track was placed, and calibrated numerical models for both situations. They concluded that the ballast superstructure provided an additional stiffness of about $22-27\%$ for the three lowest modes, and showed how the stiffness of the ballast and continuity of the track had a significant effect on the second vertical bending mode due to an apparent change in the supports behaviour.

Even though the effect of the ballast track on the dynamic response of railway bridges has already been a matter of study by scientists and engineers, in the opinion of the authors some important aspects have not yet been addressed in depth or with sufficient generality. Among them (i) stiffness and damping parameters in discrete track models used for similar track geometries greatly differ among publications. Moreover, no studies have been presented stating the effect and extent of these parameters variations; (ii) many authors disregard the shear transmission between the ballast mobilized masses, increasing the track-bridge stiffness and leading to energy dissipation; (iii) in multi-span simply-supported bridges the contribution of adjacent spans is generally disregarded and no studies have been found investigating under what circumstances the maximum acceleration

response in operating conditions may be higher when considering the track coupling between successive spans; (iv) the ballast coupling between adjacent twin decks and the influence of individual track parameters on the evolution of the natural frequencies and modal shapes in these types of bridges, especially for modes with an important transverse deformation of the cross-section, has not been investigated with the sufficient level of detail.

In this paper, the influence of the ballasted track–bridge vertical interaction on the response of railway bridges composed of SS spans is investigated, as an extension of a preliminar study performed by the authors in Moliner et al. (2020). The original contributions of the work presented herein with respect to previous investigations are: (i) focusing on the effect of ballast shear transmission mechanisms along the track and between structurally independent parts of the bridges, i.e. consecutive spans and adjacent twin decks, and on how discrete track models reproduce these phenomena; (ii) analysing the influence and extent of the different track parameters on the bridge dynamic properties and (iii) on the bridge response at resonant, not resonant and cancellation situations; (iv) detecting under what circumstances the use of single-span models for multi-span bridges may not be on the safe side; (v) validating the previous conclusions through the comparison with experimental measurements on a real structure from a conventional railway line composed of two SS spans and two twin adjacent decks per span weakly connected through the ballast.

2. Numerical models

In the range of lengths of interest (i.e. $10 - 25\,\mathrm{m}$) usual deck typologies in the Spanish railway system are solid or voided concrete slabs, prestressed concrete filler beams encased in a concrete pseudo-slab and precast decks composed of double-T beams (see Figure 2). This justifies the nature of the numerical models adopted in this investigation.

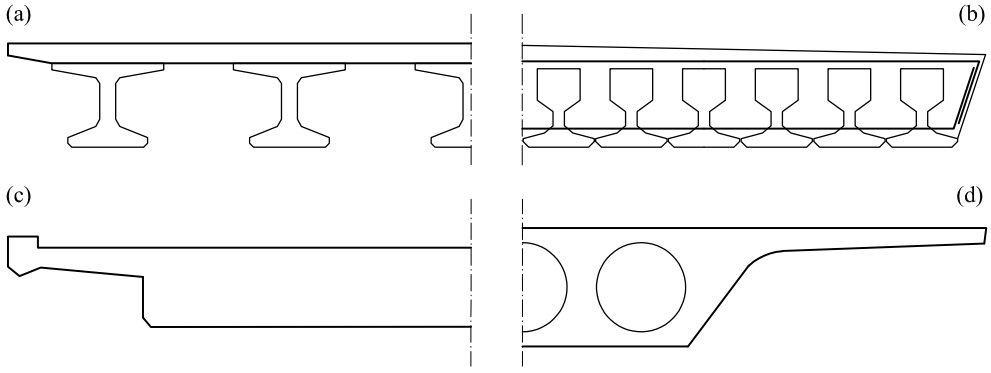

Figure 2. Common railway bridge decks for short-to-medium lengths: (a) pre-cast double-T girder deck; (b) concrete filler beam deck; (c) solid concrete slab; (d) voided concrete slab.

In the next section, the three-layer discrete track model is presented, common for the 2D and 3D FE track-bridge interaction models. In the former, the bridge deck is simulated by means of a Bernoulli-Euler (B-E) beam. This planar model is used to perform a comprehensive sensitivity analysis of the track individual parameters, and to investigate the adequacy of predicting the maximum acceleration in multi-span bridges with single-span planar models. On the other hand, in the 3D track–bridge model the deck is represented as an isotropic Kirchhoff plate, connected to B-E beams accounting for the longitudinal girders in the case of girder decks. This model is used to analyse the coupling introduced by the ballast layer along the deck borders between structurally independent parts of the bridge, i.e. adjacent twin decks and consecutive spans, and for comparison with the experimental response in the last section.

2.1. *Track model*

A three–layer discrete track model (see Figure 3) as the one proposed by Zhai et al. (2004, 2009) is adopted. The rail is modelled as a B-E beam resting on equidistant supports. The damping and vertical stiffness of the rail pads, C_p and K_p, mobilised ballast, C_b and K_b, and subgrade, C_f and K_f, are concentrated at each sleeper location. Also, to account for the interlocking among the ballast granules, vertical spring-damper elements simulating the associated shear stiffness and damping with constants K_w and C_w, are introduced to link the relative vertical displacements between adjacent ballast masses. The parameters K_f^b and C_f^b stand for the vertical subgrade stiffness and damping on the bridge deck which, in this study, is set to $100 \cdot K_f$ and 0, respectively, assuming that the ballast rests directly on the deck slab. Finally, E_r, I_{yr}, m_r stand for the rail Young Modulus, cross-section moment of inertia with respect to the Y axis defined in Figure 4 and linear mass. As can be derived from Figure 3, the track model used in this work only considers the response in the vertical plane, while the longitudinal track-bridge interaction is neglected in a first approach due to the high bending stiffness of railway bridge decks. This is consistent with recent publications that focus on the transverse dynamic response of the bridge (Cantero et al. (2016); Xiao et al. (2020)). In the absence of braking forces or temperature gradients, the coupling effects in the vertical direction prevail over those in the longitudinal one, and thus they may be evaluated in a decoupled manner (Wu et al. (2021)).

In the 2D model described in Subsection 2.2, mass, stiffness and damping coefficients as well as the rail area and moment of inertia are multiplied by a factor of 2 (as indicated in Figure 3), as only one rail is explicitly included in the model. This idealisation admits Ahlbeck hypothesis which states that the load transmitted from a sleeper to the ballast coincides approximately with a cone distribution with an inclination defined by the ballast stress pervasion angle corresponding to the Poisson ratio (Ahlbeck et al. (1978)). For the particular expressions used to calculate M_b, K_b and K_f, the reader is referred to Zhai et al. (2004). The rest of the parameters are extracted from the literature, as specified in Section 3.1.

2.2. *2D track-bridge interaction model*

In the planar model, the bridge is simulated by N_{sp} isostatic beams, where N_{sp} stands for the number of spans, resting on vertical elastic supports that represent the neoprene bearings. In Figure 3, $\bar{K}_{bi}^n$ stands for the constant equivalent vertical stiffness in each external section of the deck in the i-th bridge span. L_{bi}, E_{bi}, I_{ybi} and m_{bi} are the span length, bridge deck Young Modulus, cross-section moment of inertia with respect to the Y axis and linear mass of the i-th bridge span, respectively. The only interaction between successive spans is due to the track. A track length of $L_{r,prev} = 20\,\text{m}$ is included before and after the bridge, equivalent to more than 30 times the sleeper distance D_{sl}, which is considered adequate according to previous publications (Clark et al. (1982); Lou (2005)) and to a convergence test performed to this end.

As for the train excitation, a constant moving load model is adopted, therefore neglecting vehicle-structure interaction (VBI) and track irregularity effects. Since the main purpose of the work is the evaluation of the vertical coupling exerted by the ballasted track in consecutive spans and adjacent decks, this is a deliberate decision as (i) it is intended to isolate the effect of track components from other interaction mechanisms that can be overlapped in resonance situations; (ii) only the bridge response is of interest; (iii) VBI effects are mainly relevant at resonance (Doménech et al. (2014)); (iv) reliable data for the train suspension systems included in Section 4 are not available at the time of writing. Also, previous studies have shown that the effects of track irregularities are noticeable on the vertical response of the vehicle itself and are perceptible in the soil far away from the track, being less important for the infrastructure at the bridge site in the frequency range of interest (Peixer et al. (2021); Romero et al. (2012, 2013)). The model is implemented in ANSYS R17.1. The full mass, stiffness and damping matrices are exported to MATLAB R2017b and the equations of motion are integrated in the time domain applying the Newmark-beta constant

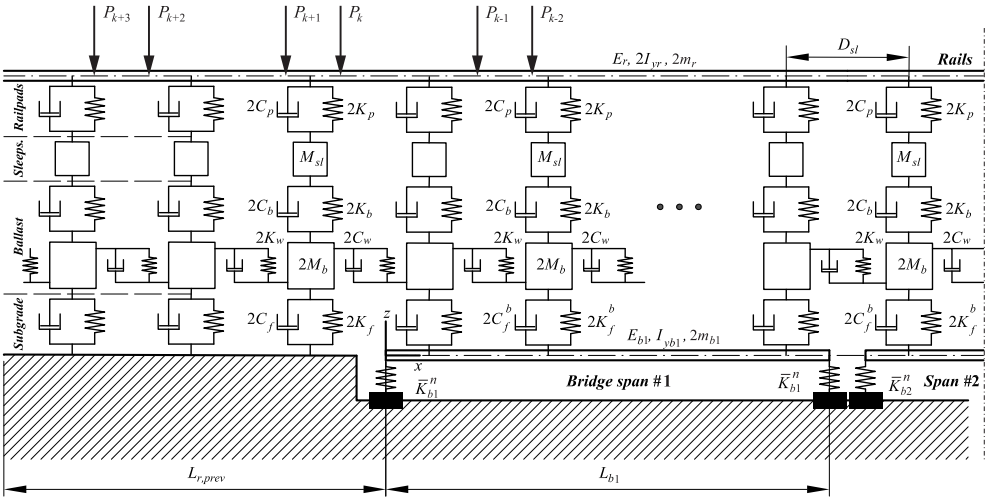

Figure 3. 2D track-bridge interaction model.

acceleration algorithm. The time step is defined as the minimum between 1/50 times the smaller period of interest and 1/20 times the travelling time of an axle load between two consecutive sleepers.

2.3. *3D track-bridge interaction model*

The 3D FE track-bridge interaction model is outlined in Figure 4. This model permits one to evaluate the ballast vertical shear transmission between single-track adjacent decks of the same span (from now on *deck coupling*) and between consecutive spans (from now on *span coupling*) through the shared ballast layer.

The main features of the model are:

- The decks are represented as isotropic Kirchhoff plates discretised into shell FE with 6 degrees of freedom (dof) per node. The element size is chosen to adequately reproduce the wavelengths of the modes with frequencies up to 30 Hz as per Eurocode (EC) CEN/TC250 (2005).
- In each slab, different mass density elements are defined in order to concentrate the weight of the nonstructural elements over the corresponding contributive areas.
- The longitudinal girders are represented as B-E beam elements with 6 dof per node. These nodes are connected to the plate through kinematic constraints. The distance between the plate and the beam nodes equals the existing vertical offset between the slab neutral plane and the center of mass of the girders.
- Vertical interaction due to the shared ballast distributed over the twin decks and between consecutive spans is simulated as discrete spring elements with stiffness constants K_{wL} and K_{wT}, respectively.
- The discrete track models adopted in the longitudinal (X) and transverse (Y) directions are represented in Figure 4. In the transverse direction, the ballast shear stiffness and damping constants are designated as K_{wr} and C_{wr}, respectively.
- The vertical stiffness of the laminated rubber bearings is included at the centre of each bearing by means of a vertical spring with elastic constant K_{bi}^n.
- As in the 2D track-bridge model, constant moving loads are adopted for the railway excitation, therefore neglecting VBI.
- To reduce computational costs, in this case the dynamic equations of motion are transformed into modal space and integrated in the time domain by the Newmark-beta linear acceleration algorithm as in Bonifácio et al. (2014); Chellini et al. (2011); Liu et al. (2014). The time-step is defined as 1/25 times the smallest period of interest.

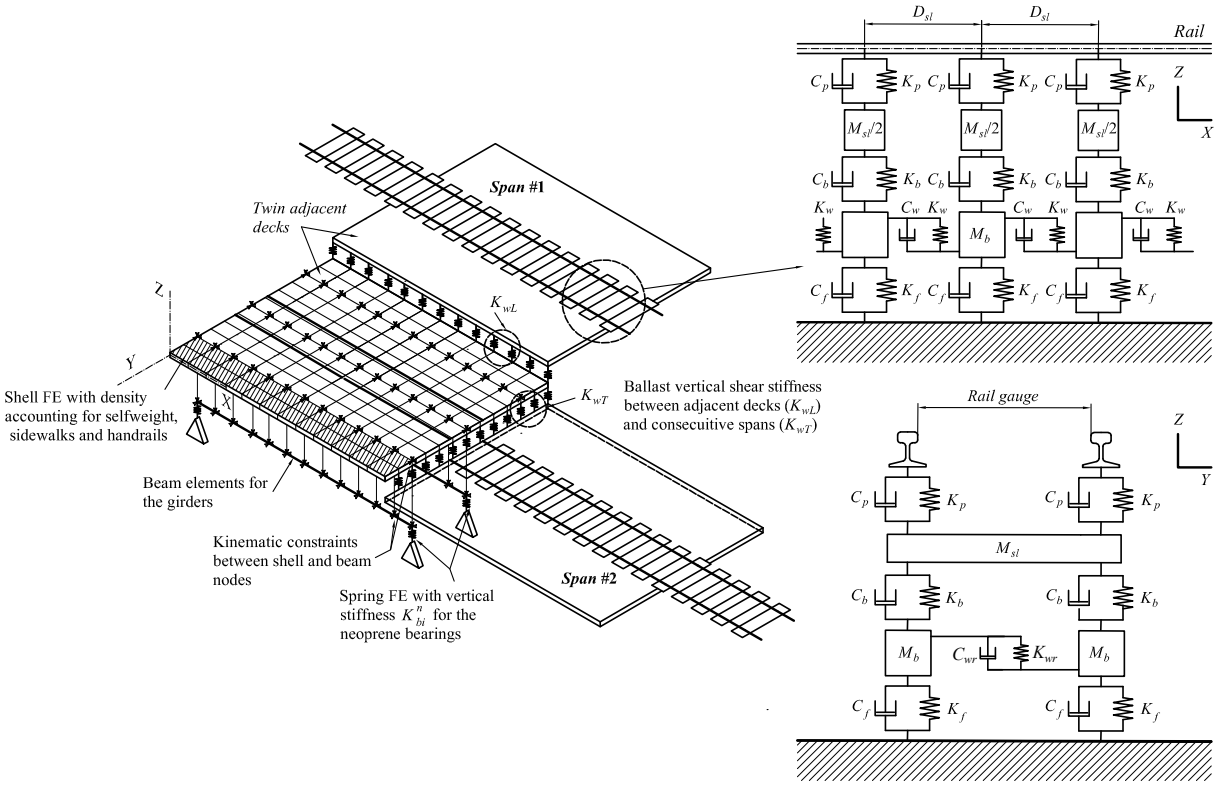

Figure 4. 3D track-bridge interaction model.

3. Sensitivity analysis of ballasted track parameters

3.1. *Track nominal parameters and methodology*

In Figure 5 the values adopted by different authors of the track parameters K_p, C_p, K_b and C_b are included. The high dispersion among the values is evident and constitutes one of the reasons for the sensitivity analysis presented in what follows. Regarding the ballast shear stiffness and damping, K_ω and C_ω, only a few references are found in the literature providing approximate values for similar track characteristics. Particularly $K_\omega \in \left[5.4 \cdot 10^7, 7.84 \cdot 10^7\right]$ N/m according to Rodrigues and Dimitrovová (2013), Zhang et al. (2017), Punetha et al. (2020), and $C_\omega = 8 \cdot 10^4$ Ns/m is most often used as in Zhai et al. (2004). First, a set of reference track parameters is defined as a basic set for subsequent studies (see Table 1). As indicated in Table 1 the majority of the parameters are calculated according to Zhai et al. (2004). This constitutes a well-established standard and it is proximate to the average of the values included in Figure 5. The rail, rail pads and sleeper properties are selected from Standards and data from the Spanish railways (CEN/TC256 (2017); Ministerio de Fomento (2010); Melis (2007); Nguyen et al. (2012)).

Two single-track bridges are analysed in this section using the 2D model from Section 2.2. The first, identified in what follows as Br-12m, corresponds to Old Guadiana River Bridge, which is a real bridge from a Spanish conventional railway line described in detail in Section 4. Old Guadiana River Bridge is made up of two identical SS spans of approximately 12 m in length. In each span the deck is composed of two adjacent structurally independent single-track decks. In this section only one of the decks is analysed neglecting any transverse coupling through the ballast between the decks. The second bridge is a variant from the former, with two identical spans of 20 m (Br-20m). In both cases, the track properties are considered identical. Table 2 includes the basic properties of the beam models that represent each of the bridges. f_1 and M_{bi} represent the fundamental frequency and the total mass per span, respectively. Br-20m bridge presents a similar static bending stiffness as Br-12m ($L_{b1}/\delta_{UIC71} = 2250$). The mass of Br-20m bridge is selected from the catalogue proposed

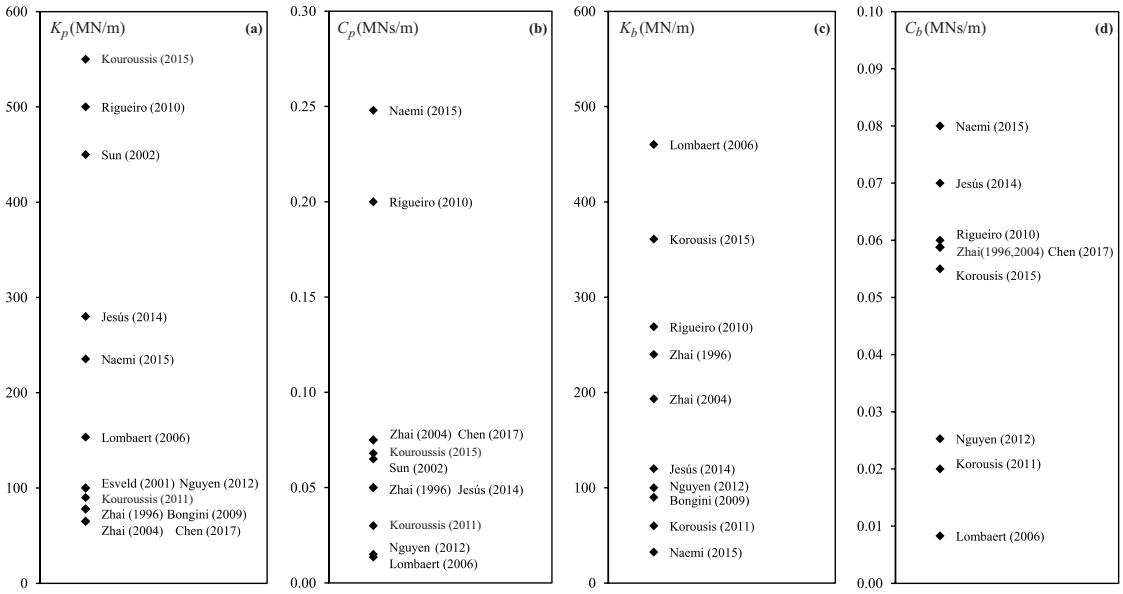

Figure 5. Rail pad and ballast layer stiffness and damping values admitted by different authors in the past for comparable ballast layers thicknesses and sleeper distances (Bongini and Poisson (2009); Chen et al. (2017); Esveld (2001); Jesús et al. (2014); Kourousis et al. (2011); Kouroussis et al. (2015); Lombaert et al. (2006); Naemi et al. (2015); Nguyen et al. (2012); Rigueiro et al. (2010); Sun and Dhanasekar (2002); Zhai (1996); Zhai et al. (2004)).

Notation	Parameter	Value	Unit	Source
E_r	Rail UIC60 elastic modulus	$2.100 \cdot 10^{11}$	Pa	CEN/TC256 (2017)
I_{yr}	Rail UIC60 moment of inertia	$3055 \cdot 10^{-8}$	m^4	CEN/TC256 (2017)
m_r	Rail UIC60 mass per unit of length	60.335	kg/m	CEN/TC256 (2017)
K_p	Rail pad vertical stiffness	$1.000 \cdot 10^8$	N/m	Nguyen et al. (2012),Melis (2007)
C_p	Rail pad damping	$7.500 \cdot 10^4$	Ns/m	Zhai et al. (2004)
M_{sl}	Sleeper mass	300	kg	Ministerio de Fomento (2010)
D_{sl}	Sleeper distance	0.600	m	Ministerio de Fomento (2010)
l_e	Half sleeper effective suporting length	0.950	m	Zhai et al. (2004)
l_b	Sleeper width	0.300	m	Ministerio de Fomento (2010)
α	Ballast stress distribution angle	35	(°)	Zhai et al. (2004)
h_b	Ballast thickness	0.300	m	Ministerio de Fomento (2010)
ρ_b	Ballast density	1800	kg/m^3	Zhai et al. (2004)
M_b	Ballast vibrating mass	317.910	kg	Zhai et al. (2004)
E_b	Balast elastic modulus	$1.100 \cdot 10^8$	Pa	Zhai et al. (2004)
K_b	Balast vertical stiffness	$1.933 \cdot 10^8$	N/m	Zhai et al. (2004)
C_b	Ballast damping	$5.880 \cdot 10^4$	Ns/m	Zhai et al. (2004)
E_f	Subgrade K_{30} modulus	$9.000 \cdot 10^7$	Pa/m	Zhai et al. (2004)
K_f	Subgrade vertical stiffness	$7.399 \cdot 10^7$	N/m	Zhai et al. (2004)
C_f	Subgrade damping	$3.115 \cdot 10^4$	Ns/m	Zhai et al. (2004)
K_w	Ballast shear stiffness	$7.840 \cdot 10^7$	N/m	Zhai et al. (2004)
C_w	Ballast shear damping	$8.000 \cdot 10^4$	Ns/m	Zhai et al. (2004)

Table 1. Track model parameters (per rail seat).

by Doménech et al. (2014) for single-track bridges of a similar typology. Concerning the vertical stiffness of the neoprene bearings, in both bridges this value is selected so that the ratio between the flexural stiffness of the bridges and the equivalent vertical stiffness of the bearings for dynamic loads $\bar{K}^n_{bi,dyn}$, is in the range shown in Equation (1), which is a common interval in this type of structures and supports according to previous works (Museros et al. (2013)). A factor of 2 is

admitted between the static and dynamic vertical stiffnesses of the bearings.

$$\kappa = \frac{E_{bi} I_{ybi} \pi^3}{\bar{K}^n_{bi,dyn} L^3_{bi}} \in [0.05 - 0.1] \tag{1}$$

Figure 6 shows the first six natural frequencies and mode shapes calculated with the 2D track-bridge interaction model described in Section 2.2 for the two bridges of study (Br-12m and Br-20m). The number of sleepers is not exactly the same in the two spans. This causes a slight asymmetry in the mode shapes, which is more evident in the case of the shortest bridge. In what follows a sensitivity analysis is performed with the aim of evaluating the influence of individual variations of the track parameters on the bridge harmonic response (Section 3.2) and under the passage of trains (Section 3.3). Finally, the effect of including a different number of spans in the 2D model on the bridge maximum response and on the most critical section is also investigated (Section 3.4).

Parameter	Unit	Br-12m	Br-20m
N_{sp}	[ ]	2	2
L_{bi}	m	11.93	20.00
f_1	Hz	10.07	6.67
M_{bi}	kg	106659	210407
$E_{bi}I_{ybi}$	MNm^2	7087	28800
$\bar{K}^n_{bi,st}$	MN/m	1116.5	1488.3

Table 2. Bridges Br-12m and Br-20m properties.

3.2. *Harmonic response*

In this section a vertical harmonic force with constant amplitude $F_0 = 210\,\text{kN}$ is applied on the rail at mid-span of the first span of the bridges. The maximum absolute vertical displacement at the same point is determined for exciting frequencies in the range $f_f \in [1, 600]$ Hz in steps of $\Delta f_f = 0.1\,\text{Hz}$. This analysis is repeated considering independent variations of the track parameters with respect to the reference ones (i.e. those included in Table 1). Figure 7 shows the results of the analysis for the Br-12m bridge. No structural damping is added, apart from that of the discrete track elements. The rail is discretised into two beam elements between consecutive sleepers, and so are the bridges. From the analysis of the results, the following is observed:

- Two relevant maxima predominate in the harmonic response: a narrow peak corresponding to resonance of the fundamental mode of the bridge deck close to 10 Hz (see Figure 6(a-b)) and a wider maximum in the vecinity of 160 Hz coinciding with the first modes with a high contribution of the track deformation. Smaller peaks stand out along the response curves coinciding with the bridge higher frequencies with non-zero amplitudes at mid-span.
- The effect of the subgrade damping (C_f) is negligible in the full frequency range. The effect of the rail pads and ballast dampings, C_p and C_b, affects the response at high frequencies but not under 60 Hz.
- The only damping parameter that significantly affects the amplitude at low frequencies is the movilised ballast shear damping C_w, leading to a decrease of the response close to the bridge fundamental frequency, as shown in Figure 7(g).
- As per the track stiffness properties, the variation of the subgrade stiffness K_f is negligible, which is expected as the ballast rests directly on the bridge slab and a very high value of K^b_f is admitted. The increase in the rail pads and ballast stiffnesses, K_p and K_b, leads to a slight decrease of the amplitude at high frecuencies and to an increase of the track resonant response close to 160 Hz but, again, it does not affect the bridge response at low frequencies.

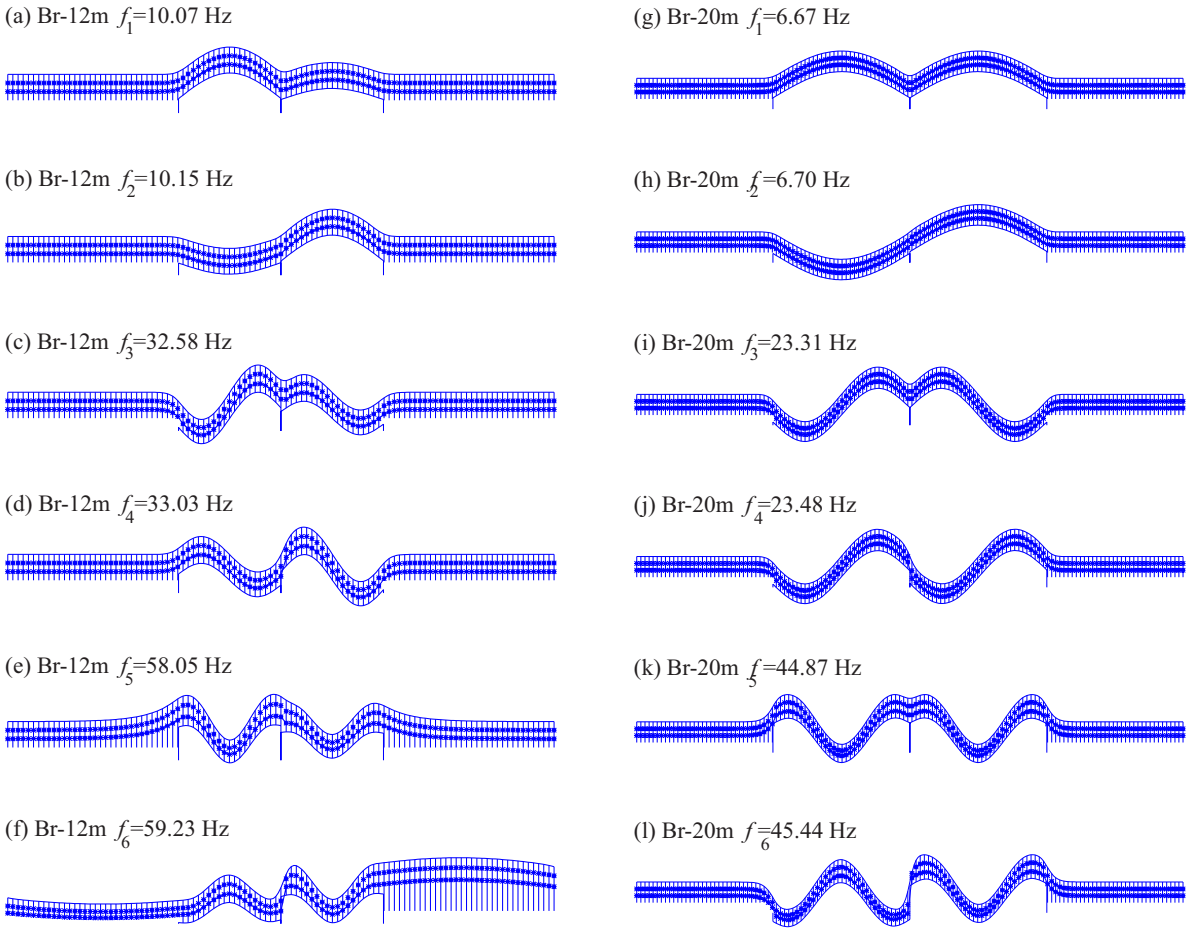

Figure 6. First six natural frequencies and mode shapes of bridges (a)-(f) Br-12m and (g)-(l) Br-20m under study.

- The only track stiffness parameter that significantly affects the response close to the bridge fundamental frequency is the shear stiffness of the movilised ballast masses K_w, leading to an increase in the resonant frequency of approximately 1 Hz in the range of variation $[0.5 - 2]\, K_w$. This is consistent with the variation of the fundamental frequency, as shown in what follows.

Similar conclusions are drawn for the Br-20m bridge. The results for this bridge are not included for the sake of conciseness. Finally, the variation of the natural frequencies for the lowest modes of both bridges are determined and represented in Figure 8 versus the ballast shear stiffness K_ω. Notice that in this figure, A stands for the factor that multiplies the nominal value of K_ω. The natural frequencies of the bridges increase with K_ω. Maximum alterations take place for the fundamental mode and the shortest bridge, for which f_1 reduces approximately 8% when $K_\omega = 0$ and increases about 7% for twice the nominal value of this parameter.

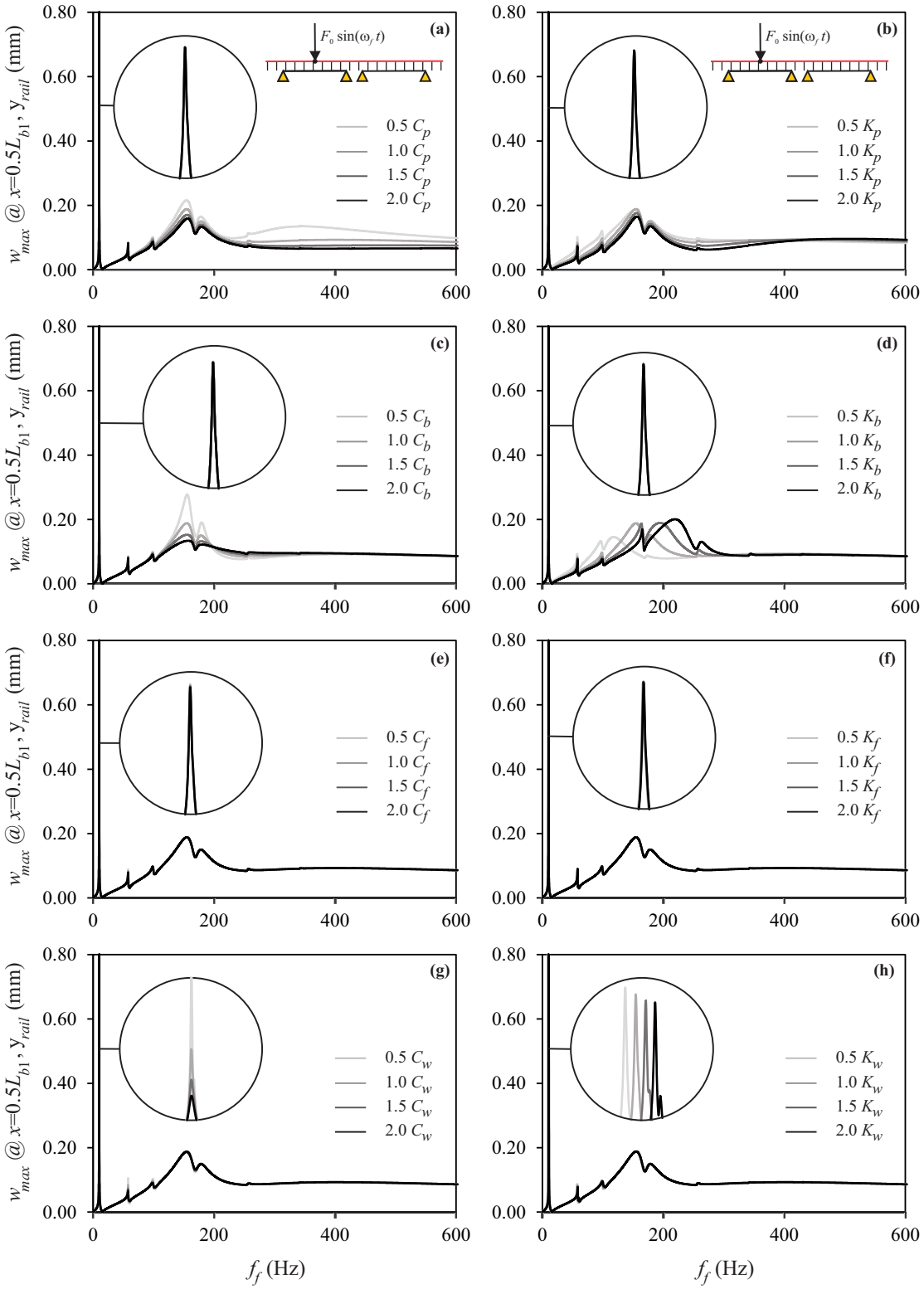

Figure 7. Br12m harmonic test results for individual variations of the track parameters.

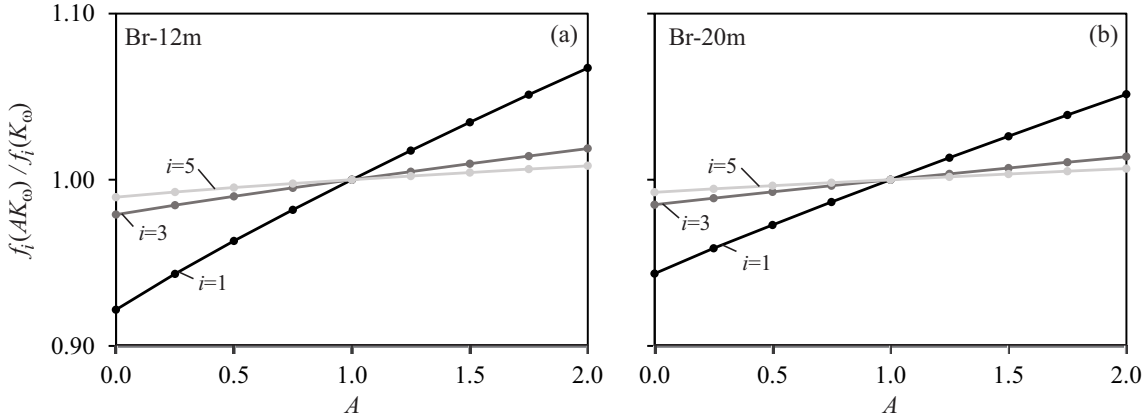

Figure 8. Frequency variations with K_ω for (a) Br-12m and (b) Br-20m bridges.

3.3. *Bridge vertical acceleration under train passages*

Next, the effect of the track parameters on the bridge maximum acceleration under trains of equidistant loads is investigated. To this end, the response of Br-12m and Br-20m bridges is obtained under the circulation of two trains of 20 equidistant loads of 210 kN. In the first case, the distance between the loads $d_k = 18$ m and in the second, $d_k = 27$ m, with the aim of inducing two clear resonances of the same order in the structures at similar speeds. The response of the bridge in terms of vertical displacement and acceleration is obtained in the time domain at $\{0.25, 0.5, 0.75\}\, L_{bi}$ of each span for 61 velocities in the range $[40, 100]$ m/s. A Chebyshev order 3 filter is applied to the acceleration response filtering contributions below 1 Hz and above 60 Hz. After filtering, maximum response envelopes are obtained for individual variations of the track parameters.

To reduce the computational cost and ensure accuracy of results at the same time, each rail element length is set as one sleeper distance and supported by two adjacent sleepers as in previous works (Wang et al. (2018)). Rayleigh damping is added accounting for structural damping according to Eurocode 1 (CEN, EN 1991-2 (2003)) for prestressed concrete bridges: 1.56% for the Br-12m bridge and 1.0% for the Br-20m bridge. These ratios are applied to the first and fifth natural frequencies. In the range of velocities considered, second, third and fourth resonances of the fundamental mode are induced. Equations (2a) and (2b) provide these velocities in the reference case for the Br-12m and the Br-20m bridges, respectively.

$$V_{1,j}^{r,Br12m} = \frac{d_k = 18\text{m} \cdot f_1 \cdot 3.6}{j} \rightarrow V_{1,2}^r = 326.3\,\text{km/h} \qquad V_{1,3}^r = 217.5\,\text{km/h} \qquad V_{1,4}^r = 163.1\,\text{km/h} \tag{2a}$$

$$V_{1,j}^{r,Br20m} = \frac{d_k = 27\text{m} \cdot f_1 \cdot 3.6}{j} \rightarrow V_{1,2}^r = 324.2\,\text{km/h} \qquad V_{1,3}^r = 216.1\,\text{km/h} \qquad V_{1,4}^r = 162.1\,\text{km/h} \tag{2b}$$

In Figure 9 the acceleration envelopes for the Br-12m bridge at the centre of the second span are represented versus the train speed considering independent variations of the track parameters. As predicted, three resonances are induced in the vicinity of the theoretical ones. From the analysis of the results the following is observed:

- The effect of rail pads and ballast damping parameters, C_p and C_b, is negligible on the bridge acceleration response in the full range of velocities (see Figure 9(b-d)).
- The bridge maximum acceleration at resonance reduces slightly as the rail pads stiffness, K_p, decreases. This effect is more visible at higher-order resonances (see Figure 9(a)). The effect

of this parameter far from resonance is almost imperceptible. The evolution of the response with the movilised ballast stiffness, K_b, follows the same trend although it is less evident (see Figure 9(c)).

- The two parameters that affect the most the bridge response are the ballast shear stiffness and damping, K_w and C_w, which is consistent with the results obtained from the previous section. As K_w increases, so does the bridge fundamental frequency and, consequently, the resonant speeds (see Figure 9(e)). Increasing C_w leads to a pronounced reduction of the bridge response at resonance (see Figure 9(f)). Far from resonance, the effect of this parameter is limited. It should be stressed that a wide range of variations of damping and stiffness track parameters have been considered in this analysis to magnify their effect.

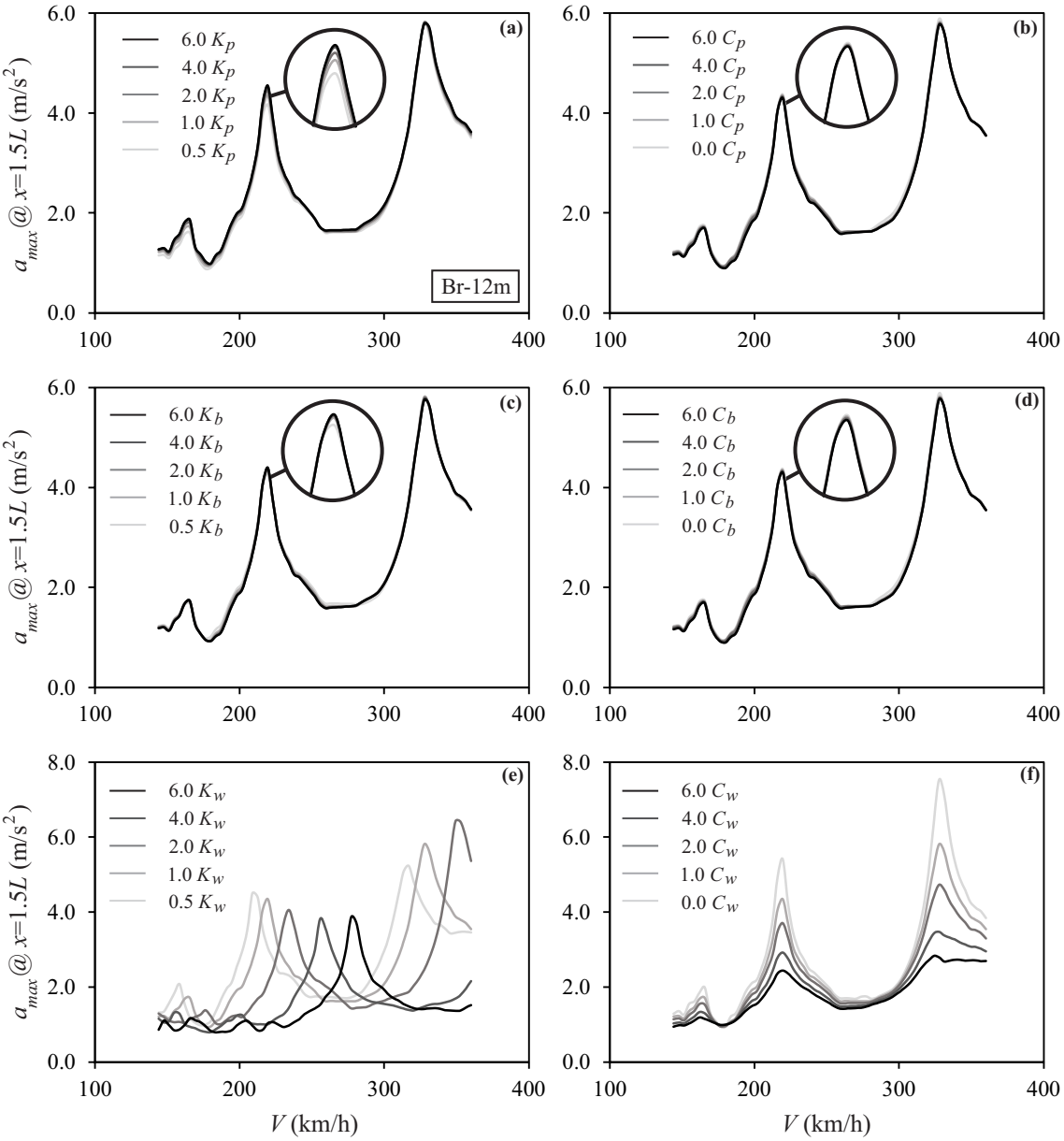

Figure 9. Br-12m bridge maximum vertical acceleration vs. train speed for independent variations of track parameters.

Figure 10 shows the same results for the Br-20m bridge under the action of the train with

$d_k = 27$ m. In this case, the second resonance, which for the particular characteristic distance should occur close to 324.2 km/h according to Equation (2b), does not take place. This is a consequence of the particular ratio $L_{bi}/d_k = 0.74$ that leads to the cancellation of the second resonance of the fundamental mode in elastically-supported beams (for the particular flexibility of the neoprene bearings, i.e. $\kappa = 0.075$, this ratio is 0.7192 according to Martínez-Rodrigo et al. (2020); Museros et al. (2013)). Despite the presence of the track, the phenomenon of cancellation of resonance still takes place for L_{bi}/d_k ratios similar to those derived for simple beams. As for the effect of the track parameters, the same trends in the bridge response are detected. Nevertheless, it should be said that the reduction of the response at resonance with decreasing values of K_p and K_b is almost imperceptible now. Regarding the alteration of the resonant speed with K_w, this is proportional to the alteration in the bridge fundamental frequency shown in Figure 8.

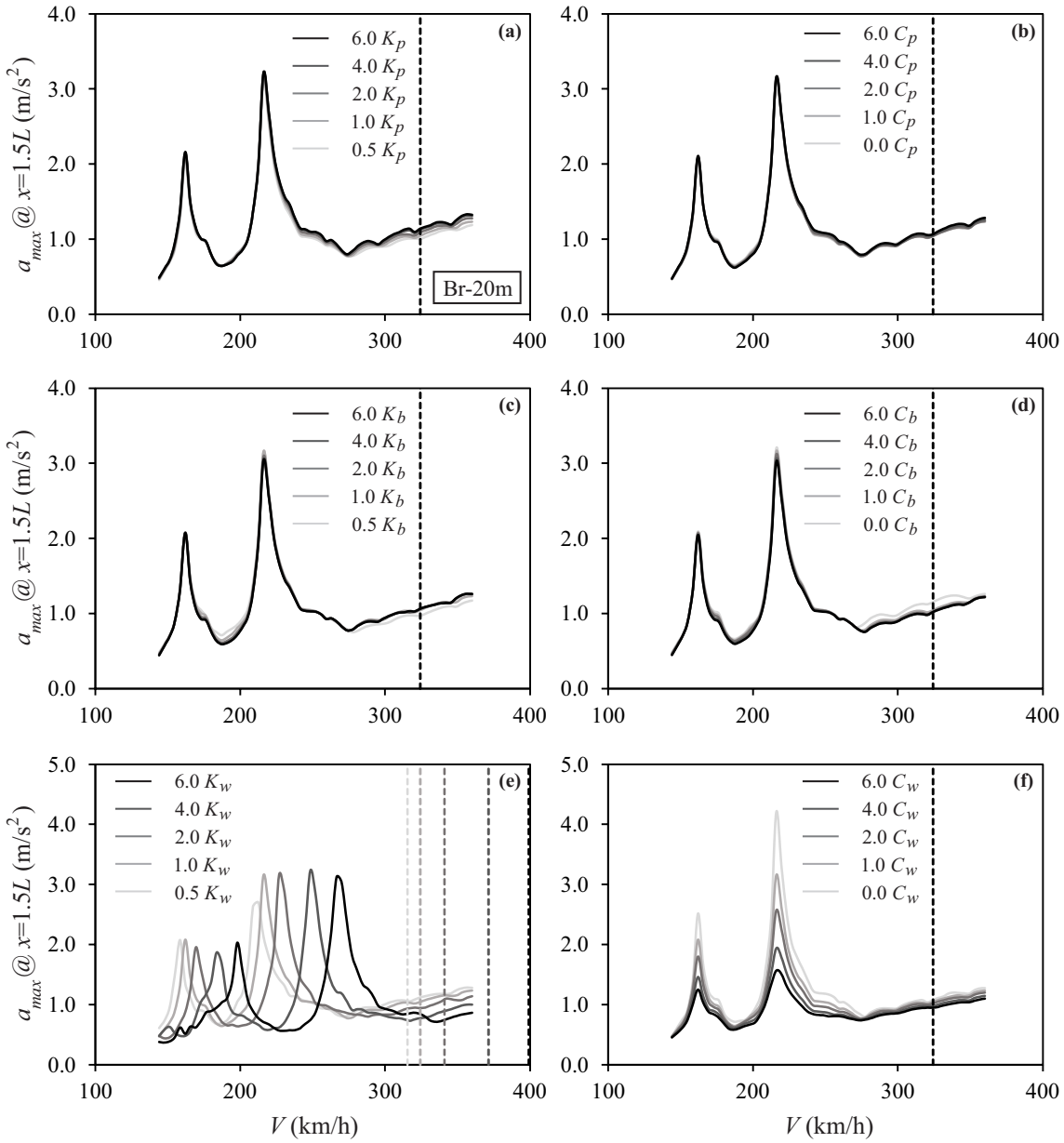

Figure 10. Br-12m bridge maximum vertical acceleration vs. train speed for independent variations of track parameters.

3.4. *Influence of the number of spans on the bridge maximum response*

In this section, the influence of the number of spans on the maximum acceleration under train passages in multi-span structures is investigated. Due to the longitudinal coupling exerted by the track between the structurally independent spans, the maximum response and the section where it takes place may differ depending on the number of spans considered. The analysis is performed for Br-12m and Br-20m bridges in two cases: considering and neglecting the vertical flexibilities of the neoprene bearings. The maximum acceleration is now obtained at nine sections per span with $0.10 \cdot L_{bi}$ spacing. The bridges are analysed under the same equidistant trains with $d_k = 18\,\text{m}$ and $d_k = 27\,\text{m}$ in the range $[40, 100]$ m/s in 1 m/s steps. In Figure 11 the magnitude $\bar{a}_{max}$ is plotted in each section where

$$\bar{a}_{max}(x) = \frac{a_{max}(x)}{a_{max}^{1sp}} \tag{3}$$

In Equation (3), a_{max}^{1sp} indicates the overall maximum acceleration (considering the complete range of velocities and all the post-process bridge sections) predicted by the model with one span, and $a_{max}(x)$ is the maximum acceleration considering the complete range of velocities at a particular section x predicted by the model with either two or three spans, neglecting or considering the vertical flexibility of the neoprene bearings. In Figure 11, plots (a) and (c) show the maximum response predicted by the two-span models of the Br-12m and Br-20m bridges, respectively; and plots (b) and (d) correspond to the three-span models of both bridges. In all the graphs, dark gray (ES) and light gray (SS) columns represent $\bar{a}_{max}$ considering or neglecting the vertical flexibility of the neoprene bearings, respectively. Notice that values higher than $\bar{a}_{max} = 1$ indicate sections where the maximum acceleration calculated with more than one span exceeds the value predicted with the one-span models.

In the Br-12m case the maximum acceleration given by the one-span model takes place at mid-span in both the ES and the SS cases. When the flexibility of the neoprene bearings is taken into account, the model with two spans predicts a maximum acceleration that exceeds by 18% that given by the one-span model, and takes place at mid-span of the second span. Similar results are obtained in the case of three spans: the most critical section is $1.6 \cdot L_{b1}$, and the maximum response is 16% higher than that given by the one-span model. On the other hand, in the SS case the maximum response is predicted at the mid-span section of the first span, both when two and three spans are included, and the maximum acceleration predicted by the one-span model is only exceeded by approximately $5 - 6\%$. In the Br-20m case, similar trends are observed. When the supports are considered elastic, the models with two or three spans predict a level of acceleration 17% and 20% higher than that resulting from the one span model, respectively; also, in the former cases the most critical section belongs to the second and third spans, respectively. When the spans are considered SS, a minor difference is observed between the number of spans, and the maximum acceleration only exceeds by 7% the maximum value provided by the one-span model.

Therefore, from the results presented herein it is concluded that when the track is included (i) models with only one span may not predict the maximum overall vertical acceleration in multi-span bridges; and (ii) the difference in the amplitude of the maximum response between spans is higher when the vertical flexibility of the bearings is taken into account. It could be of interest to extend the study to other lengths and bridge deck typologies with different flexural stiffnesses.

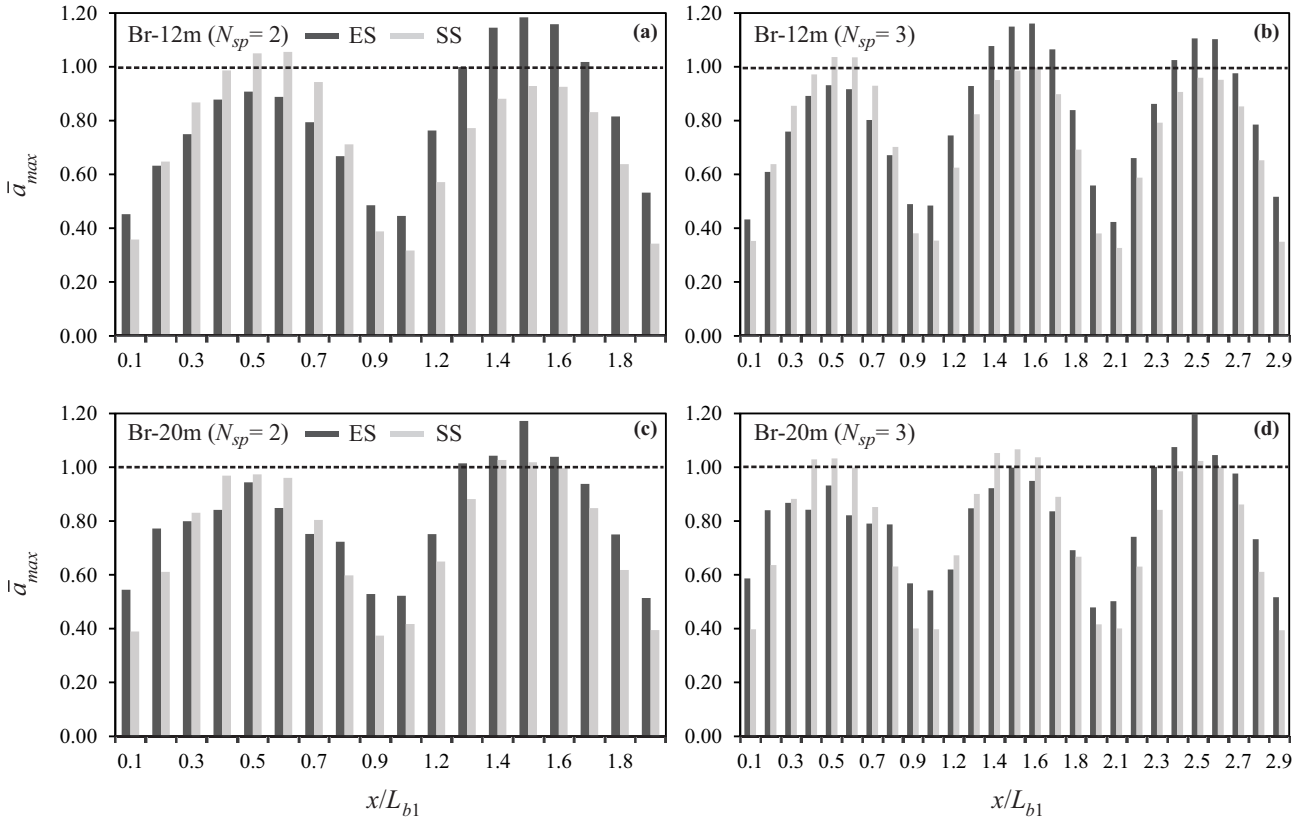

Figure 11. $\bar{a}_{max}$ vs. bridge x coordinate for Br-12m bridge with (a) 2 spans and (b) 3 spans; $\bar{a}_{max}$ vs. bridge x coordinate for Br-20m bridge with (c) 2 spans and (d) 3 spans.

4. Ballast vertical coupling along the deck borders

In this section, the vertical coupling induced by the shared ballast along the deck borders, i.e. between adjacent decks of the same span and between consecutive spans, is investigated. The study is centered on the real structure Old Guadiana River Bridge which consists of two identical SS spans with twin adjacent single-track decks. The deck width of this bridge is common in single track decks of Spanish conventional lines and the span length is representative of short bridges which may experience important acceleration levels under operating conditions. In what follows, the bridge and the experimental campaign carried out by the authors with the purpose of characterising the structure dynamic properties is described. Then, the 3D numerical model presented in Section 2.3 is updated to reproduce the experimental modal properties. Especial attention is paid to the vertical shear transmission through the ballast between decks and spans. Finally, the experimental response of the bridge under the passage of real trains is discussed and compared with the predictions of the calibrated numerical model.

4.1. *Case study: Old Guadiana River Bridge*

The Old Guadiana River Bridge belongs to the conventional railway line Madrid-Alcázar de San Juan-Jaén, in Spain. It is a double-track concrete bridge with two identical simply-supported bays with 11.93 m of span length (Figure 12). The horizontal structure is formed by two adjacent but structurally independent decks, composed of a reinforced concrete slab resting on five prestressed concrete rectangular girders (see Figure 13). Each deck accommodates a ballasted track with Iberian gauge UIC60 rails and mono-block concrete sleepers at regular distances of 0.60 m. The longitudinal girders of the decks rest on the two abutments and on a central support through laminated rubber

bearings.

Figure 12. Old Guadiana River Bridge.

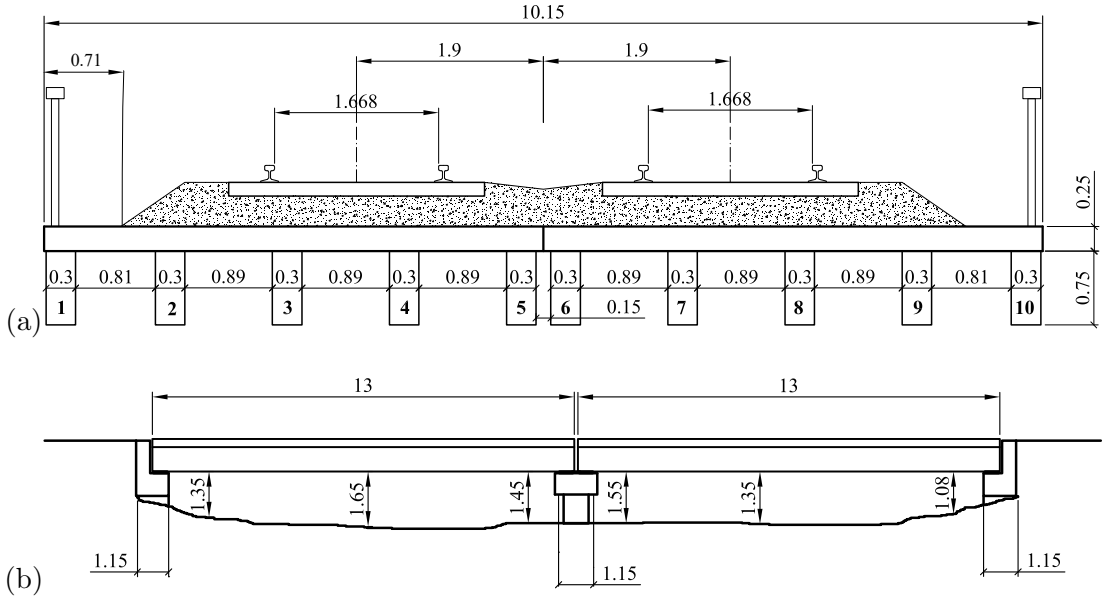

Figure 13. Old Guadiana River Bridge: (a) Cross section of the deck; (b) Lateral view.

In May 2019, the authors conducted an experimental campaign with the aim of characterising the dynamic response of the structure and the surrounding soil. For a detailed description of the experimental campaign the reader is referred to Galvín et al. (2021). Vertical acceleration was measured under ambient and train-induced vibration at 18 points of the lower horizontal face of the pre–stressed concrete girders (points 1-18 in Figure 14). Ambient vibration data recorded for 3600 s were used for the identification of the modal parameters of the bridge using state-space models. Additionally, modal damping ratios were also identified from the free vibrations left by the train passages, using 10 s of the acquired signals. As indicated in Galvín et al. (2021), the technique described by Kim et al. (2005) was used, which is based in the following three steps: (i) first, a digital band-pass filter is used to isolate each of the natural frequencies of interest from the free vibration time history signals. The pass bands of the digital filter are determined from the frequency content of the recorded accelerations. Special attention is paid to avoid overlapping when the natural frequencies are proximate; (ii) once the mode shapes are identified, single-degree of freedom responses that represent the response of the structure in each mode of vibration are obtained; (iii) the damping ratios are determined by fitting an exponential decay function to the single-degree of freedom responses.

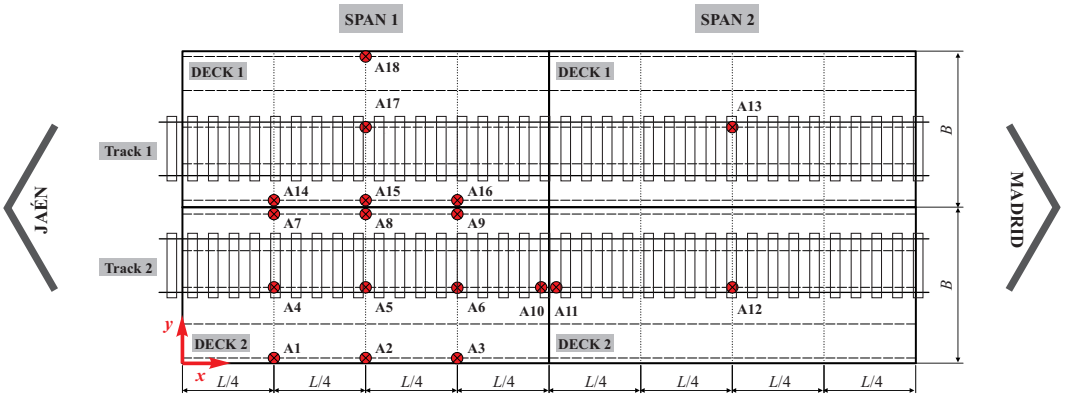

Figure 14. Old Guadiana River Bridge sensors layout.

Table 5 shows the damping ratios (ζ_{exp}) and the natural frequencies of the five identified modes (f_{exp}). The mode shapes are represented in Figure 15 in a solid black trace. The lowest one in frequency order corresponds to the first longitudinal bending of each bay where the two adjacent decks vibrate in phase. The second mode is the first torsion mode of the connected decks. In the third mode, the two adjacent decks deform under independent torsion but out of phase such that they conform a combined first transverse bending mode. In the aforementioned modes, the coupling due to the ballast layer connecting the adjacent decks is very evident. The fourth and fifth modes correspond, to an in-phase torsional deformation and to the transverse bending of each independent deck, respectively.

Mode	1	2	3	4	5
f_i^{exp} [Hz]	9.84	11.03	12.84	21.43	28.74
ζ_i^{exp} [%]	2.8	2.6	1.5	1.5	1.0

Table 3. First five frequencies and modal damping ratios identified experimentally.

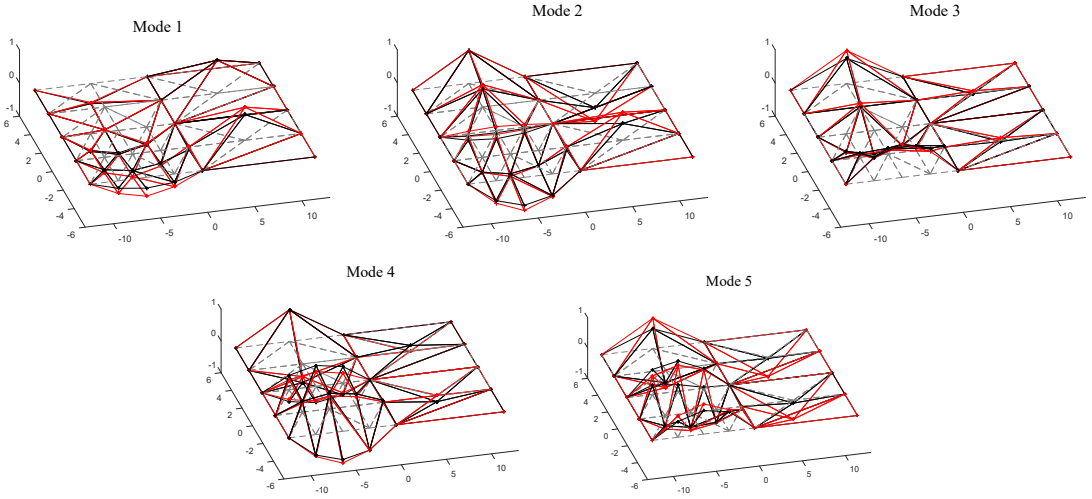

Figure 15. Identified mode shapes (black solid line) vs. calibrated (red solid line) on the Old Guadiana River Bridge. Undeformed shape (dashed gray line).

4.2. *Model updating from experimental measurements*

First, the 3D track-bridge interaction model is updated in order to reproduce the natural frequencies and mode shapes identified experimentally. This procedure is performed in two steps: (i) a preliminary sensitivity analysis to identify the most influencing parameters of the model, and (ii) the updating of these parameters through an automated iterative procedure for the minimisation of an objective function by means of a genetic algorithm. Table 4 lists the main parameters, including the initial values, ranges of variation, and the final (updated) values. The choice of the initial values, lower and upper bounds is based on engineering considerations, the level of uncertainty and on reference values found in the literature, cited in the last column. In the table, E and ρ refer to the elastic modulus and mass density of the slab and the girders. Since no information was available on the material properties of the old Guadiana River Bridge, typical values for reinforced concrete have been adopted as initial guesses and a reasonable range of variation is admitted for the elastic modulus. The parameters I_{yg} and J_g stand for the second moment of area and the torsional constant of the girders cross-section, respectively. These properties have been estimated from the bridge technical drawings and are not included in the updating process. Concerning the track parameters, for the sake of brevity, in Table 4 only the parameters that may differ from those previously presented in Table 1 are listed: the ballast thickness underneath the sleepers h_b, the vibrating ballast mass M_b and immobilised mass m_b, and the ballast shear stiffness along each rail K_w and between rails K_{wr}. For the remaining track parameters, the reference values listed in Table 1 are used and are not included in the updating process.

	Notation	Initial value	Optimisation range	Calibrated value	Unit	Source
Slab	ρ_s	2500	-	2500	[kg/m^3]	Malveiro et al. (2018)
	E_s	36000	[-20,+10]%	39390	[MPa]	Malveiro et al. (2018)
Girders	I_{yg}	0.011	-	0.011	[m^4]	
	J_g	0.005	-	0.005	[m^4]	
	ρ_g	2500	-	2500	[kg/m^3]	Malveiro et al. (2018)
	E_g	36000	[-20,+10]%	30127	[MPa]	Malveiro et al. (2018)
Track	h_b	0.32	[0.3, 0.45]	0.32	[m]	Ministerio de Fomento (2010)
	M_b	317.9		349.256	[kg]	Zhai et al. (2004)
	m_b	584.702		581.882	[kg/m^2]	
	K_w	$7.84 \cdot 10^7$	[-30, +30] %	$5.49 \cdot 10^7$	[N/m]	Zhang et al. (2017)
	K_{wr}	$7.84 \cdot 10^7$	[0, +30] %	$1.65 \cdot 10^4$	[N/m]	
Coupling parameters	K_{wL}	$1.31 \cdot 10^8$	[0, +30] %	$2.76 \cdot 10^7$	[N /m^2]	
	K_{wT}	$1.31 \cdot 10^8$	[0, +30] %	$1.00 \cdot 10^5$	[N /m^2]	
Supports	$K^n_{bi,st}$	$2.23 \cdot 10^8$	-	$2.23 \cdot 10^8$	[N/m]	
	$K^n_{bi,dyn}$	$2.45 \cdot 10^8$	[1.1, 2]$\times K^n_{bi,st}$	$4.46 \cdot 10^8$	[N/m]	Manterola (2006)

Table 4. Mechanical properties of the 3D track-bridge interaction FE model.

As shown in Section 3.3 the ballast shear stiffness along the track K_w may significantly affect the bridge response, but information about realistic values for this parameter is scarce. Thus, a wide range of variation is admitted centered on the value proposed by Zhai et al. (2004). K_{wr} represents the ballast shear transmission in the transverse direction. For this variable, the lower bound is reduced to 0 as the gauge distance is almost four times the sleeper distance. The same initial values and ranges of variation are assumed for the ballast shear stiffnesses along the borders of the deck, i.e. between consecutive spans and adjacent decks, K_{wT} and K_{wL}, which are unknown and one of the main focus of this research. Since these discrete springs are distributed along the deck edges, the corresponding stiffnesses are given per unit length in Table 4, with the initial value set to $K_w/D_{sl} = 7.84 \cdot 10^7/0.6 = 1.31 \cdot 10^8$ N/m^2. Concerning the vertical stiffness of the neoprene bearings for static loads, an initial value $K^n_{bi,st} = 2.23 \cdot 10^8$ N/m is calculated from a pre-design, as no information about the dimensions or mechanical properties of the bearings was available. Then, the stiffness under dynamic loading $K^n_{bi,dyn}$ is updated by multiplying the static

value by a factor in the range [1.1,2] according to Manterola (2006). Eight parameters are chosen as possible candidates for the updating process: E_s, E_g, h_b, K_w, K_{wr}, k_{wL}, k_{wT} and $K^n_{bi,dyn}$. In order to avoid a poorly conditioned optimisation problem, a sensitivity analysis is performed to identify the parameters that most influence the prediction of the natural frequencies and mode shapes, in terms of frequency differences between the experimental (f_i^{exp}) and paired numerical modes (f_i^{num}) (Equation (4)) and Modal Assurance Criterion (MAC) numbers (Equation (5)).

$$e_i = \frac{f_i^{exp} - f_i^{num}}{f_i^{exp}} \tag{4}$$

$$\mathrm{MAC}_i = \frac{\left((\Phi_i^{exp})^{\mathrm{T}}\Phi_i^{num}\right)^2}{\left((\Phi_i^{exp})^{\mathrm{T}}\Phi_i^{exp}\right)\left((\Phi_i^{num})^{\mathrm{T}}\Phi_i^{num}\right)} \tag{5}$$

In the previous equation Φ_i^{exp} and Φ_i^{num} are the i-th experimental mode and the paired numerical counterpart associated with mode i, and superscript T indicates transpose. The sensitivity analysis is performed using the Latin Hypercube sampling technique. 500 samples are generated within the ranges presented in Table 4 and the Spearman linear correlation matrix between the model parameters and the frequency differences and MAC numbers is computed. Figure 16 shows the correlation matrix for the first three modes. The coefficients +1 or -1 imply a perfect monotone correlation. In the graphs, coefficients between -0.25 and +0.25 are excluded from the graphical representation.

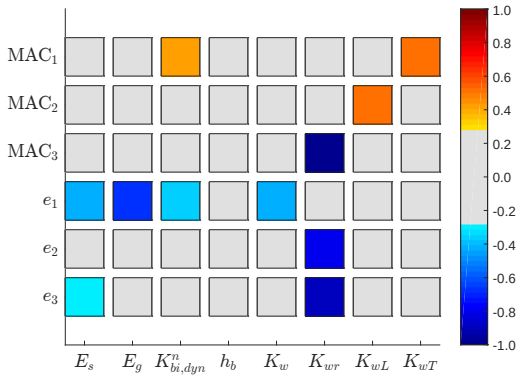

Figure 16. Spearman linear correlation matrix between model parameters and modal properties

As can be seen, all the selected model parameters have a clear influence on the natural frequencies and mode shapes for the ranges of variations considered, the ballast height h_b being comparatively the least influencing parameter. It is also noticeable that the ballast coupling parameters K_{wL} and K_{wT} are especially relevant for an accurate calibration of the first and second modes in terms of MAC numbers. As a second step in the updating process an automated optimisation procedure is implemented in ANSYS-MATLAB for the minimisation of the objective function F_{obj}, defined in Equation (6), applying a genetic algorithm. Based on the Spearman correlation matrix, seven model parameters are updated (E_s, E_g, K_w, K_{wr}, K_{wL}, K_{wT} and $K^n_{bi,dyn}$). The ballast height h_b is assumed constant and set equal to its nominal value $h_b = 0.32\,\mathrm{m}$. The ranges of variation of the parameters are again those given in Table 4.

$$F_{obj} = \sum_{i=1}^{n} |e_i| + \sum_{i=1}^{n} (1 - \mathrm{MAC}_i) \tag{6}$$

The objective function F_{obj} involves both natural frequencies and MAC numbers for a total number of n identified modes. In this study the first three modes are included in the optimisation range, due to their predominant contribution to the dynamic response of the bridge under operating conditions, as will be seen in Subsection 4.4. The values of the updated parameters after several runs of the genetic algorithm to guarantee the stability of the updating procedure are included in Table 4. In each run, a population size of of 70 individuals (10 times the number of calibration parameters) and 200 generations are considered. The crossover and mutation rates are set to 0.8 and 0.02, respectively, the tournament probability to 0.7, and the scale of mutation to 0.1.

The numerical frequencies, frequency differences, and MAC numbers obtained with the updated model are provided in Table 5, for the first five identified modes. Figure 15 shows, in solid red trace, the paired numerical mode shapes. The correlation with the experimental measurements is accurate, especially for the first three modes.

Parameter/Mode	1	2	3	4	5
f_i^{num} [Hz]	9.83	10.82	13.02	19.48	27.89
f_i^{exp} [Hz]	9.84	11.03	12.84	21.43	28.74
e_i [%]	0	1.92	-1.45	9.09	2.94
MAC [-]	0.96	0.93	0.98	0.95	0.78

Table 5. Numerical and experimental natural frequencies, frequency differences, and MAC numbers for the paired modes.

4.3. *Effect of the ballast shear coupling along the deck borders on the modal parameters*

As indicated by the Spearman correlation matrix (Figure 16), the introduction of the ballast shear stiffness along the longitudinal joint (i.e., between adjacent decks of the same span), K_{wL}, is essential to reach an accurate correlation of mode 2 (first torsion mode) in terms of MAC number. A similar coupling mechanism could have been expected between consecutive spans, however it is noticeable that the difference between the updated value of the parameters K_{wL} and K_{wT} is significant. Clearly, the vertical coupling exerted by the interlocking ballast granules along the deck borders is softer between consecutive spans.

For a better understanding of the influence of K_{wL} and K_{wT} on the bridge natural frequencies and mode shapes, Figure 17 shows the results of a sensitivity analysis in which the aforementioned parameters vary independently with respect to the calibrated values from Table 4, in the range $\left[0, 1 \cdot 10^4\right] \times K_{wL}$ and $\left[0, 1 \cdot 10^4\right] \times K_{wT}$. For each variation, the frequency differences e_i along with the MAC values are calculated. A logarithmic scale is used in the horizontal axis of the plots for a better visualization of the results.

In Figure 17(a-b) the results of the model calibration under variations of the ballast shear interaction between adjacent decks of the same span (K_{wL}) are shown. The effect of K_{wL} is significant for the calibration of the second and fourth identified modes, which are antisymmetric with respect to the longitudinal axis of the bridge and thus are more influenced by structural deformability in the transverse direction. For low values of K_{wL} the numerical model is not able to properly reproduce the second and fourth modes, and the paired numerical modes exhibit low MAC numbers and high frequency differences (10% and 40%, respectively). The increase in the shear stiffness K_{wL} improves the calibration of these modes in terms of both frequencies and MAC numbers, and there exists an optimum value of this parameter for best calibrated MAC and numerical frequencies. The calibrated value ($1.0 \times K_{wL}$ =$2.76 \cdot 10^7$ N/m^2) provides accurate numerical frequencies with reasonably good MAC numbers for these two modes. For the first and third modes, a satisfactory mode pairing is achieved that is not influenced by the coupling between adjacent slabs.

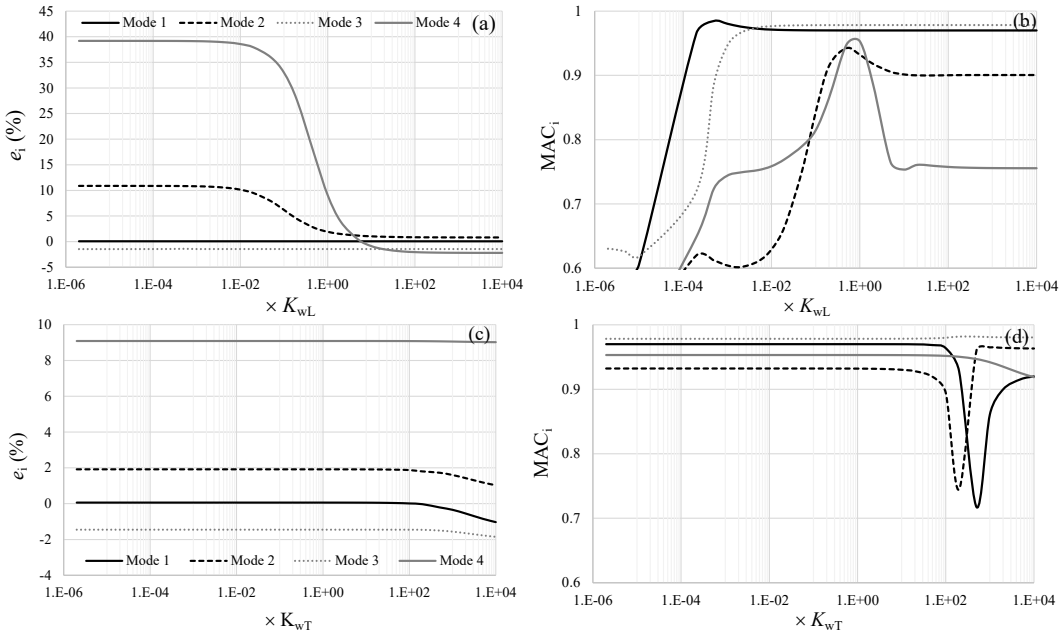

Figure 17. Sensitivity analysis on the influence of the ballast shear coupling parameters K_{wL} and K_{wT} on the natural frequencies and MAC values.

Figures 17(c-d) show the isolated contribution of K_{wT} on the model calibration. It is noticeable that the increase in K_{wT} worsens the MAC numbers for the paired mode associated to the first and second identified eigenforms after a certain threshold value, while its influence on the natural frequencies is minor. The influence of the vertical shear transfer mechanism due to the shared ballast layer between independent spans is less relevant than between adjacent decks. In any case, it is worth noting that the discrete ballast representation used in this work presents limitations and, in view of the significant dynamic coupling between the decks exhibited by this bridge, it would be of interest to continue investigating on the dynamic behaviour of this type of bridges with structurally independent parts coupled through the ballast using continuous models.

4.4. *Dynamic response under operating conditions*

During the experimental campaign, the response of the structure was recorded under the circulation of several passenger trains. The performance of the bridge was adequate from a serviceability perspective, as the maximum acceleration did not exceed the Serviceability Limit State for traffic safety in ballasted tracks, limited to 3.5 m/s^2 per European Standards (CEN/TC250 (2005)). Two of the trains are included in this section, corresponding to the medium distance Renfe trains Altaria Talgo VI and S449. Both trains crossed the bridge along track 2 (see Figure 14) northbound (Manzanares-Alcázar de San Juan). Figure 18 shows photographs of the trains and the axle scheme. Table 6 includes the arrangement of the axles and loads for each train.

Train	N	d_k[m]	l_1 [m]	l_2 [m]	P_1 [kN]	P_2 [kN]	P_3 [kN]
Altaria	7	13.14	3.44	3.3	225	70	140
S449	3	17.75	14.8	–	161	–	–

Table 6. Features of the Renfe medium distance Altaria Talgo VI and S449 trains.

The circulation speeds were identified from the frequency associated with the bogie distance as approximately 155 km/h in both cases. According to the distance between shared axles or bogies in the passenger cars, d_k, this speed is close to a third resonant speed of the fundamental mode for

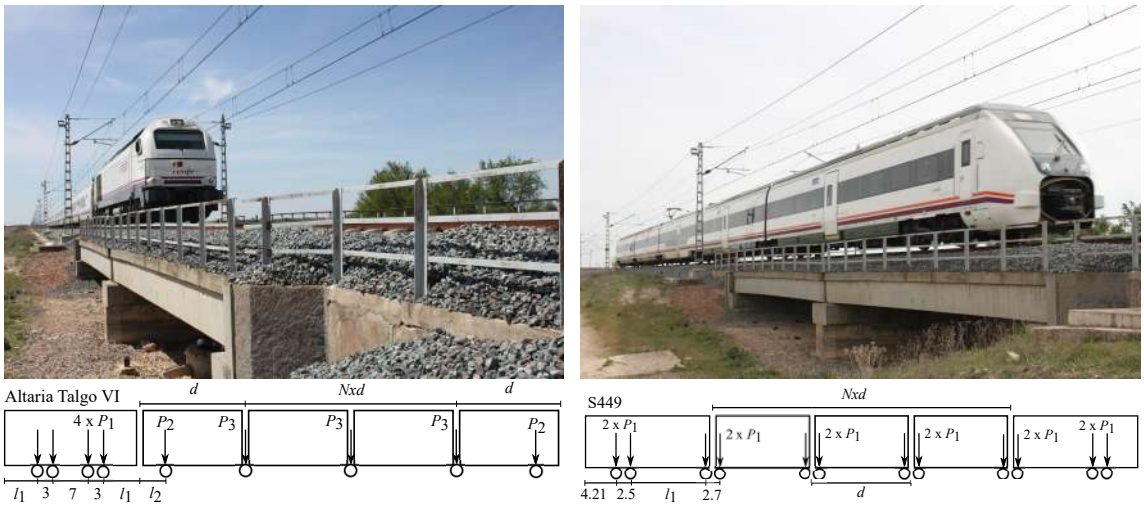

Figure 18. Renfe Altaria Talgo VI (left) and S449 (right) trains crossing Old Guadiana River Bridge

Altaria and to a fourth resonant speed of the same mode for the S449 train (Equations (7a) and (7b), respectively). Additionally, the speed of the S449 train is also in the vicinity of the theoretical critical speed for a fifth resonance of the third identified mode (Equation (7c)).

$$V_{1,3}^{r,Altaria} = \frac{13.14\,\text{m} \cdot f_1 \cdot 3.6}{3} = 155.16\,\text{km/h} \tag{7a}$$

$$V_{1,4}^{r,S449} = \frac{17.75\,\text{m} \cdot f_1 \cdot 3.6}{4} = 157.19\,\text{km/h} \tag{7b}$$

$$V_{3,5}^{r,S449} = \frac{17.75\,\text{m} \cdot f_3 \cdot 3.6}{5} = 164.01\,\text{km/h} \tag{7c}$$

The response of the bridge under the circulation of the aforementioned trains is now calculated using the numerical model updated in the previous section. The dynamic equations of motion are solved by mode superposition. Modal damping values identified during the experimental campaign under free vibration after train passages are assigned to the paired numerical modes (see Table 5).

Figure 19 shows an experimental vs. numerical comparison of the vertical acceleration at sensors 2, 5, 18 and 17 under the passage of Altaria Talgo VI train in the time (a-d) and frequency (e-h) domains. The sensors are located at mid-span under the loaded deck (a, e, b, f) and under the adjacent unloaded deck (c, g, d, h) of the same span. In all the plots the experimental signal, plotted in solid black trace, is filtered applying two third-order Chebyshev filters with high-pass and low-pass frequencies of 1 Hz and 30 Hz, respectively. The numerical predictions, plotted in gray trace, include modal contributions up to 30 Hz.

As can be depicted from the frequency domain plots, the vertical acceleration of the bridge is affected by several modal contributions, which can be attributable to the span length–to–width ratio that causes the bridge behaviour to differ from a beam-type structure. However, the peak amplitude associated to the fundamental mode predominates when compared to other modal responses, as expected in a resonance situation. This is especially evident at points 5 and 17, located at mid-span under the loaded and unloaded tracks, respectively. The response also presents visible peaks at low frequencies (in the range 3 Hz - 6 Hz) associated to the excitation and coinciding with the axle passing frequency and its multiples, which are more visible at the sensors installed under the loaded deck (points 2 and 5). For sensors 17 and 18, located at the unloaded deck, the response is still relevant (the maximum acceleration at sensor 17 reaches approximately 35% of the peak amplitude in the analogous loaded sensor number 5). This is clearly a consequence of the vibration transmission through the ballast between the two independent decks, which is evident

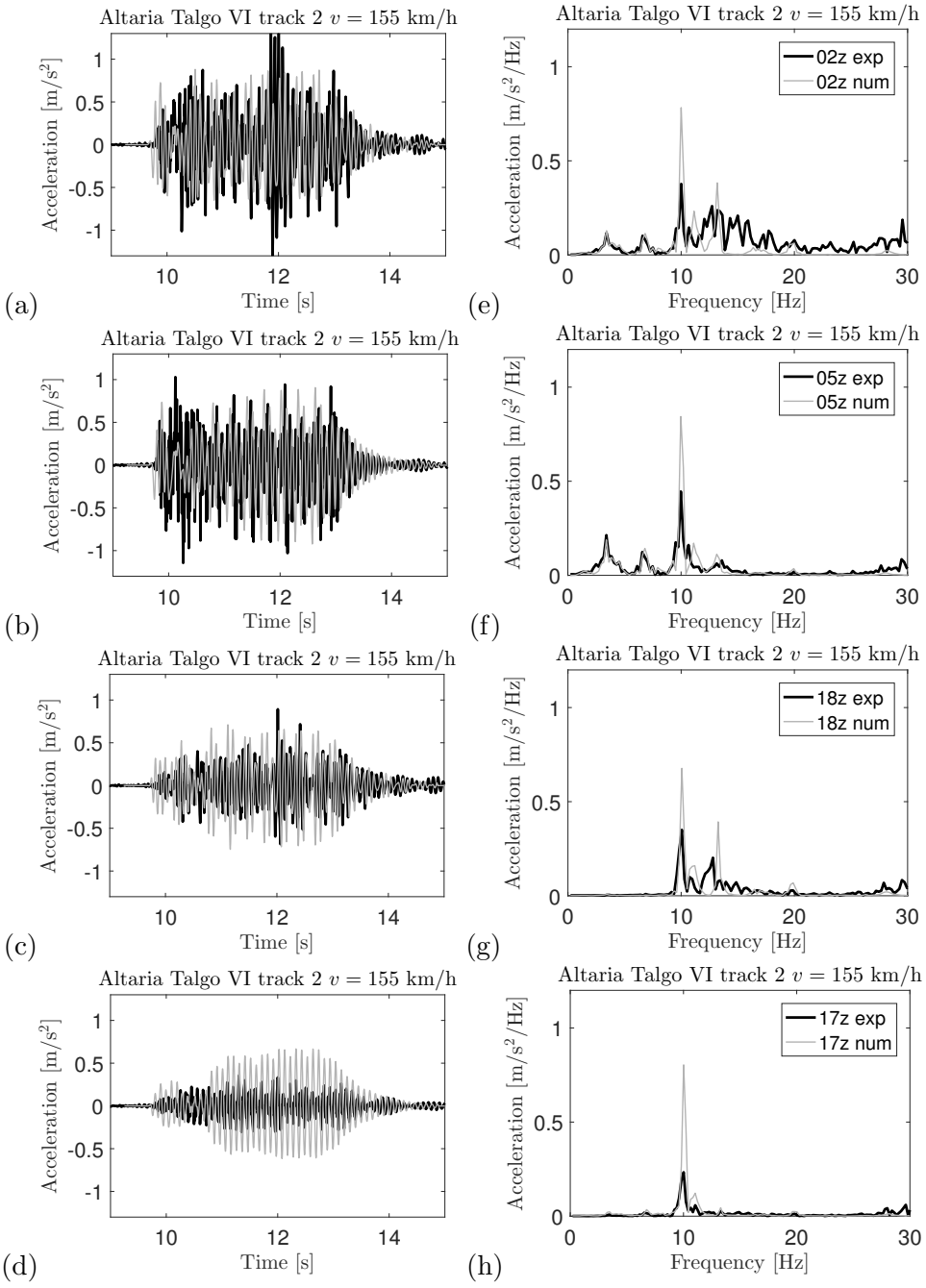

Figure 19. Old Guadiana Bridge: (a-d) time history and (e-h) frequency content of the acceleration at points 2, 5, 18 and 17 induced by Renfe Altaria train circulating along track 2. Experimental results (black line) vs. numerical predictions (gray line)

both under ambient and under forced vibrations, despite the difference in amplitude between these two situations.

The numerical predictions seem reasonable, especially for the sensor located at mid-span in the loaded deck (sensor 5) and in the frequency range of interest. The contribution of mode 1 prevails in all the sensors located under the loaded track (sensors 5, 4 and 6, the latter not shown in the plots) and is to some extent overestimated by the numerical model. This could be attributable to the interaction between the bridge and the vehicle suspension systems, not included in the model and more relevant in a resonance situation. The response at the same locations but measured under the unloaded track, sensors 17 and 13 (the latter not visible in Figure 19), reveals also

certain overestimation of the acceleration content associated to the fundamental mode. This is more noticeable during the forced-vibration phase, according to the corresponding time-domain plots (Figure 19(d)). Conversely, the acceleration amplitude is accurately predicted in the unloaded deck during the free-vibration phase, entailing an accurate identification of structural damping for comparable amplitudes of vibration. This difference in the numerical and experimental adjustment between the forced and free vibration phases may be related not only to VBI but also to amplitude-dependent damping mechanisms and other sources of nonproportional local damping, such as the ballast shear damping along the track and between the ballast-connected structures. For the sensors located at the external borders of both decks (sensors 2 and 18) the participation of several mode contributions below 30 Hz is significant, especially that of the second (first torsion) and third (first transverse bending) modes. This stresses the need to simulate the coupling exerted by the track in these types of structures. Nevertheless, the contribution of the fundamental mode on these sensors responses prevails, as a consequence of the first mode resonance induced by Altaria Talgo.

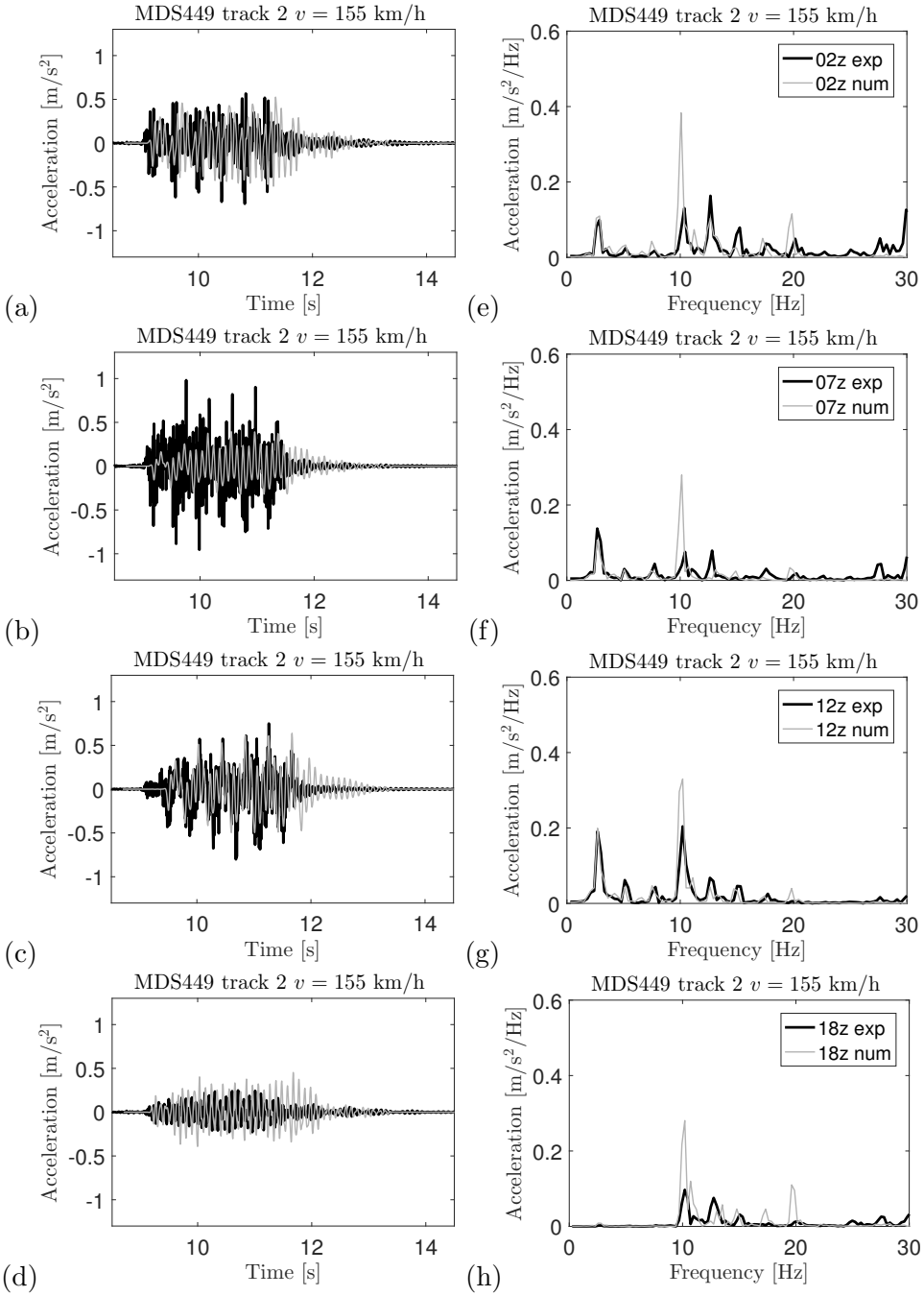

Figure 20. Old Guadiana River Bridge: (a-d) time history and (e-h) frequency content of the acceleration at points 2, 7, 12 and 18 induced by Renfe train S449 circulating on track 2. Experimental results (black line) vs. numerical predictions (gray trace)

Figure 20 shows the vertical acceleration response of the bridge under the passage of Renfe train S449. In this case, new sensors are included in the plots for a better interpretation of the bridge behaviour, in particular sensors 2 and 7. Sensors 12 and 18 are again chosen for comparison with the previous train. During this train passage the predominant contribution of the fundamental mode is not so evident, and the response at the third bridge modal frequency (12.8 Hz) is easily distinguishable in all the recordings. This is consistent with the fact that train S449 may excite a fourth resonance of the fundamental mode and a fifth resonance of the third mode (Equations (7b-c)). Given the high order of both resonances, which implies that the structure experiences more

cycles of vibration in the absence of loads, the associated peaks are visible but a clear predominance in the frequency response does not occur, contrarily to the response under the previous train passage. At sensors 2, 7 and 18, given their positions close to the deck border, the peaks associated to the first and third identified frequencies present similar amplitudes; and at sensor 12, located under the loaded track close to the deck centre, the frequency contribution of the first mode is more relevant. It is noticeable that the vertical acceleration levels induced by S449 are lower than those associated to Altaria Talgo shown in Figure 19. This may be attributable to the higher resonance order (four cycles of oscillation of the bridge between consecutive bogies instead of three) and the smaller number of passenger coaches in S449 train (3 vs. 7). Furthermore, the peak amplitudes associated with excitation (v/d_k =2.5 Hz and multiples) are also more visible in the sensors installed under the loaded deck and even higher at some positions than the peaks associated with the bridge lowest natural frequencies, which can also be associated to the lower number of coaches and the particular axle arrangement of S449, in which two axles act simultaneously in the same span with a total static load of $2P_1 = 322\,\text{kN}$.

As in the previous train passage, the vibration amplitude at the unloaded deck (sensor 18) is also substantial (the maximum acceleration is in this case 44% of the highest level measured in sensor 2) and reveals the coupled dynamic behaviour of the twin decks. The numerical model in this case is able to reproduce the real response of the bridge more accurately than in the previous case, both at the loaded and unloaded decks, despite the fact that several modes contribute to the response. Clearly, the bridge behaviour differs substantially from that of a beam-type structure, and the need of a structurally more complex model with a fine representation of modes with transverse deformation of the cross-section is needed. In this regard, the coupling exerted by the ballast track, especially along the longitudinal joint, plays an important role. At the fundamental mode, there is still certain over-prediction of the experimental acceleration due to the interaction phenomena not included in the model but, nevertheless, the 3D numerical model captures the majority of the frequency contributions in the frequency range of interest with a very reasonable computational cost.

5. Conclusions

This work focuses on ballast vertical shear transmission mechanisms that take place in railway bridges composed of structurally independent decks sharing a common ballast layer, i.e. single-track twin decks and bridges with simply-supported spans. The main interests are assessing the effect on the dynamic response of the bridges of such weak coupling, and the adequacy of using discrete track models to tackle this phenomenon. Two types of track-bridge interaction analyses are performed. First, using a 2D model, a comprehensive sensitivity analysis on independent variations of the parameters of a well-established discrete track model is performed, and the adequacy of predicting the maximum acceleration of multi-span bridges with single-span models is critically evaluated, the only means of connection between the spans being the discrete ballasted track. Second, using a 3D model, the ballast vertical shear transmission mechanism that takes place along the deck borders in bridges composed of single-track twin decks and SS spans sharing a common ballast layer is investigated. In this case the study focuses on a representative but particular structure. The model is updated by means of a genetic algorithm and the effect of the ballast vertical coupling on the modal properties and the dynamic response under operating conditions is evaluated. The main conclusions of the study are:

- Within the range of variation of the track parameters, the only two parameters that can significantly affect the bridge response at low frequencies are the ballast shear stiffness and the damping. The bridge natural frequencies increase with K_ω. Maximum alterations occur for the fundamental mode and the shortest bridge. An increase of C_ω leads to an important reduction of the bridges resonant response and its effect is negligible when far from resonance.

- Despite the presence of the track, the phenomenon of cancellation of resonance still takes place for similar L_{bi}/d_k ratios as those derived for simple elastically-supported beams.
- When using planar track-bridge interaction models, models with only one span may not predict the maximum overall vertical acceleration in multi–span bridges. Also, the difference in the maximum response between spans is greater when the vertical flexibility of the bearings is taken into account. In the bridges analysed, this difference reaches 20%. An intensive analysis of track parameters covering a wide range of lengths and typologies of bridges of interest would be valuable for future studies.
- Regarding the analysis of the Old Guadiana River Bridge, there exists a significant dynamic coupling between the consecutive spans and, especially, between the twin adjacent decks, which can be detected under both ambient and train-induced vibrations despite the difference in amplitude. This effect could be attributable to the continuity of the ballasted track.
- An adequate fitting of the experimentally identified natural frequencies and mode shapes is only achieved when discrete vertical springs representing the ballast shear transmission are included along the shared longitudinal border of the adjacent slabs, the vertical coupling between consecutive spans exerted by the ballast layer and the track continuity having a lower influence in the model calibration.
- Discrete track models, despite their limitations, may be an interesting alternative when representing the dynamic response of ballast-connected structures, counterbalancing accuracy and computational cost. Nevertheless, an experimental and reliable quantification of the track stiffness parameters that these models include is needed.

Acknowledgements

The authors would like to acknowledge the financial support provided by the Spanish Ministry of Science and Innovation under research project PID2019-109622RB; FEDER Andalucía 2014-2020 Operational Program for project US-126491; Generalitat Valenciana under research project AICO2021/200; Junta de Andalucía and the European Social Fund through the contract USE-20617-D with the Universidad de Sevilla, and the Andalusian Scientific Computing Centre (CICA).

References

Ahlbeck D, Meacham H, Prause R (1978) The development of analytical models for railroad track dynamics. In: Kerr A (ed) Railroad Track Mechanics and Technology, Pergamon Press, pp 239–263

Bongini E, Poisson F (2009) Ground vibrations simulation cases parameters. In: Technical Report SNCF, France

Bonifácio C, Ribeiro D, Calçada R, Delgado R (2014) Dynamic behaviour of a short span filler-beam railway bridge under high-speed traffic. In: Proc. 2nd Int. Conf. on Railway Technology: Research, Development and Maintenance

Bornet L, Andersson A, Zwolski J, Battini J (2015) Influence of the ballasted track on the dynamic properties of a truss railway bridge. Structure and Infrastructure Engineering 11(6):796–803

Cantero D, Arvidsson T, O'Brien E, Karoumi R (2016) Train-track-bridge modelling and review of parameters. Structure and Infrastructure Engineering 12(9):1051–1064

CEN, EN 1991-2 (2003) Eurocode 1: Actions on Structures - Part 2: Traffic loads on bridges. European Committee for Standardization, Brussels

CEN/TC250 (2005) Eurocode: Basis of structural design. Annex A2: Application for bridges. Final version. European Committee for Standardization, Brussels

CEN/TC256 (2017) EN 13674-1:2011+A1:2017 Railway applications - Track - Rail - Part 1: Vignole railway rails 46 kg/m and above. European Committee for Standardization, Brussels

Chellini G, Nardini L, Salvatore W (2011) Dynamical identification and modelling of steel-concrete composite high-speed railway bridges. Structure and Infrastructure Engineering 7(11):823–841

Chen Z, Zhai W, Wang K (2017) A locomotive-track coupled vertical dynamics model with gear transmissions. Vehicle System Dynamics 55(2):244–267

Clark R, Dean P, Elkins J, Newton S (1982) An invesigation into the dynamic effects of railway vehicles running on corrugated rails. Journal of Mechanical Engineering Science 24(2):65–76

Doménech A, Museros P, Martínez-Rodrigo M (2014) Influence of the vehicle model on the prediction of the maximum bending response of simply-supported bridges under high-speed railway traffic. Engineering Structures 72:123–139

Esveld C (2001) Modern railway track. M.R.T.-Productions

Ministerio de Fomento GdE (2010) Instrucción de acciones a considerar en puentes de ferrocarril. Actions in railway bridges [in Spanish]

Frýba L (2008) Dynamic behaviour of bridges due to high-speed trains. In: Workshop for high-speed railways, in: Bridges for High-Speed railways, CRC Press, pp 137–158

Galvín P, Romero A, Moliner E, De Roeck G, Martínez-Rodrigo M (2021) On the dynamic characterisation of railway bridges through experimental testing. Engineering Structures 226:111,261

Galvín P, Romero A, Moliner E, Connolly D, Martínez-Rodrigo M (2021) Fast simulation of railway bridge dynamics accounting for soil-structure interaction. Bulletin of Earthquake Engineering

Hoorpah W (2008) Dynamic calculations of high-speed railway bridges in france: some case studies. In: Delgado R, Calcada R, Goicolea JM, Gabaldon F (eds) Dynamics of High-Speed Railway Bridges, CRC Press, pp 9–14

Jahangiri M, Zakeri A (2017) Dynamic analysis of train-bridge system under one-way and two-way high-speed train passing. Structural Engineering and Mechanics 64(1):33–44,

Jesús A, Dimitrovová Z, Silva M (2014) A statistical analysis of the dynamic response of a railway viaduct. Engineering Structures 71:244–259

Kim BH, Stubbs N, Park T (2005) A new method to extract modal parameters using output-only responses. Journal of Sound and Vibration 282(1):215–230

Kouroussis G, Gazetas G, Anastasopoulos I, Conti C, Verlinden O (2011) Discrete modelling of vertical track-soil coipling for vehicle-track dynamics. Soil Daynamics and Earthquake Engineering 31:1711–1723

Kouroussis G, Connolly D, Alexandrou G, Vogiatzis K (2015) The effect of railway local irregularities on ground vibration. Transportation Research Part D 39:17–30

Liu K, Lombaert G, Roeck GD (2014) Dynamic analysis of multispan viaducts with weak coupling between adjacent spans. Journal of Bridge Engineering-ASCE 19(1):83–90

Lombaert G, Degrande G, Kogut J, François S (2006) The experimental validation of a numerical model for the prediction of railway induced vibrations. Journal of Sound and Vibration 297:512–535

Lou P (2005) A vehicle-track bridge interaction element considering vehicle's pitching effect. Finite Elements in Analysis and Design 41:397–427

Malveiro J, Ribeiro D, Sousa C, Calçada R (2018) Model updating of a dynamic model of a composite steel-concrete railway viaduct based on experimental tests. Engineering Structures 164:40–52

Manterola J (2006) Puentes: apuntes para su diseño, cálculo y construcción. Servicio de Publicaciones del Colegio de Caminos, Canales y Puertos [in Spanish]

Martínez-Rodrigo M, Moliner E, Romero A, Galvín P (2020) Maximum resonance and cancellation phenomena in orthotropic plates traversed by moving loads: Application to railway bridges. International Journal of Mechanical Sciences 169:105,316

Melis M (2007) Embankments and ballast in high speed rail. fourth part: High-speed railway alignments in spain (1). certain alternatives [in spanish]. Revista de Obras Públicas (3.476):41–66

Melo LT, Malveiro J, Ribeiro D, Calçada R, Bittencourt T (2020) Dynamic analysis of the train-bridge system considering the non-linear behaviour of the track-deck interface. Engineering Structures 220:110,980

Moliner E, Romero A, Sánchez-Quesada J, Martínez-Rodrigo M, Galvín P (2020) Vertical coupling effect of the ballasted track on the dynamic behavior of multitrack railway bridges composed by adjacent decks. In: Papadrakakis M, Fragiadakis M, Papadimitriou C (eds) EURODYN 2020: XI International Connference on Structural Dynamics. Proceedings, Volume I, Institute of Structural Analysis and Antiseismic Research, School of Civil Engineering, National Technical University of Athens (NTUA), pp 1666–1679

Museros P, Moliner E, Martínez-Rodrigo M (2013) Free vibrations of simply-supported beam bridges under moving loads: Maximum resonance, cancellation and resonant vertical acceleration. Journal of Sound and Vibration 332:326–345

Naemi M, Zakeri J, Esmaeili M, Mehrali M (2015) Dynamic response of sleepers in a track with uneven rail irregularities using a 3d vehicle-track model with sleeper beams. Archives of Applied Mechanics 85:1679–

1699
Nguyen K, Goicolea J, Gabaldón F (2012) Comparison of dynamic effects of high-speed traffic load on ballasted track using simplified two-dimensional and full three-dimensional model. Journal of Rail and Rapid Transit 228(2):128–142
Peixer M, Montenegro P, Carvalho H, Rineiro D, Bittencourt T, Calçada R (2021) Running safety evaluation of a train moving over a high-speed railway viaduct under different track conditions. Engineering Failure Analysis 121:105,133
Punetha P, Nimbalkar S, Khabbaz H (2020) Analytical evaluation of ballasted track substructure response under repeated train loads. International Journal of Geomechanics 20(7):04020,093
Rauert T, Bigelow H, Hoffmeister B, Feldmann M (2010) On the prediction of the interaction effect caused by continuous ballast on filler beam railway bridges by experimentally supported numerical studies. Engineering Structures 32:3981–3988
Rebelo C, Silva L, Rigueiro C, Pircher M (2008) Dynamic behaviour of twin single-span ballasted railway viaducts. field measurements and modal identification. Engineering Structures 30:2460–2469
Rigueiro C, Rebelo C, Silva L (2006a) Vibration assessment of railway viaducts under real traffic using bridge-track models. In: Press TU (ed) Computational Methods in Engineering and Science, Springer Berlin Heidelberg
Rigueiro C, Rebelo C, Silva L (2006b) Vibration of the railway track-viaduct system under moving vehicles taking into account the interaction effect. In: Munck MD (ed) ISMA 2006: Noise and vibration engineering, Katholieke Universiteit Leuven, Department of Mechanical Engineering
Rigueiro C, Rebelo C, Silva L (2010) Influence of ballast models in the dynamic response of railway visducts. Journal of Sound and Vibration 329:3030–3040
Rocha J, Henriques A, Calçada R (2012) Safety assessment of a short span railway bridge for high-speed traffic using simulation techniques. Engineering Structures 40:141–154
Rocha J, Henriques A, Calçada R (2014) Probabilistic safety assessment of a short span high-speed railway bridge. Engineering Structures 71:99–111
Rodrigues A, Dimitrovová Z (2013) Optimization of the ballast layer in high-speed railway tracks with genetic algorithms. In: Dimitrovová Z, de Almeida JCGR, de Moura R (eds) Proceedings of the 11th International Conference on Vibration Problems (ICOVP-2013), AMPTAC, pp 1–13
Romero A, Galvín P, Domínguez J (2012) Comportamiento dinámico de viaductos cortos considerando la interacción vehículo-vía-estructura-suelo. Revista Internacional de Métodos Numéricos para Cálculo y Diseño en Ingeniería [in Spanish] 28(1):55–63
Romero A, Solís M, Domínguez J, Galvín P (2013) Soil-structure interaction in resonant railway bridges. Soil Dynamics and Earthquake Engineering 47:108–116
Sun Y, Dhanasekar M (2002) Influence of the railway track parameters to the vertical and lateral impact. In: Conference on Railway Engineering, Wollongong
Ticona L, Ribeiro D, Calçada R, Bittencourt T (2020) Validation of a vertical train–track–bridge dynamic interaction model based on limited experimental data. Structure and Infrastructure Engineering 16(1):181–201
Wang Y, Dimitrovová Z, Yau J (2018) Dynamic responses of vehicle ballasted track interaction system for heavy haul trains. In: MATEC Web of Conferences 148, 05004, EDP Sciences - Web of Conferences
Wu Q, Sun Y, Spiryagin M, Cole C (2021) Railway track longitudinal force model. Vehicle System Dynamics 59(1):155–170
Xiao X, Yan Y, Hu Z (2020) Effect of random structural damage on vehicle-track-bridge coupled response. International Journal of Damage Mechanics 29(1):103–125
Zacher M, Baeþler M (2008) Dynamic behaviour of ballast on railway bridges. In: Delgado R, Calcada R, Goicolea JM, Gabaldon F (eds) Dynamics of High-Speed Railway Bridges, CRC Press
Zakeri A, Shadfar M, Feizi M (2014) Sensitivity analysis of bridge-track-train system to parameters of railway. Latin American Journal of Solids and Structures 11(4):598–612
Zangeneh A, Battini J, Pacoste C, Karoumi R (2019) Fundamental modal properties of simply supported railway bridges considering soil-structure interaction effects. Soil Dynamics and Earthquake Engineering 121:212–218
Zhai W (1996) Two simple fast integration methods for large -scale dynamic problems in engineering. International Journal for Numerical Methods in Engineering 39(24):4199–4214
Zhai W, Wang K, Lin J (2004) Modelling and experiment of railway ballast vibrations. Journal of Sound and Vibration 270:673–683

Zhai W, Wang K, Cai C (2009) Fundamentals of vehicle-track coupled dynamics. Vehicle System Dynamics 47(11):1349–1376

Zhai W, Han Z, Chen Z, Ling L, Zhu S (2019) Train-track-bridge dynamic interaction: a state-of-the-art review. Vehicle System Dynamics 57(7):984–1027

Zhang X, Zhao C, Zhai W (2017) Dynamic behavior analysis of high-speed railway ballast under moving vehicle loads using discrete element method. International Journal of Geomechanics 17(7):04016,157